1	Measurement report: Observational insights into the impact of dust
2	transport on atmospheric dicarboxylic acids in ground region and free
3	troposphere
4	Minxia Shen ¹ , Weining Qi ¹ , Yali Liu ^{1,2} , Yifan Zhang ^{1,2} , Wenting Dai ^{1,3} , Lu Li ¹ , Xiao Guo ¹ ,
5	Yue Cao ^{1,2} , Yingkun Jiang ^{1,2} , Qian Wang ¹ , Shicong Li ¹ , Qiyuan Wang ^{1,3} , Jianjun Li ^{1,3*}
6	
7	¹ State Key Laboratory of Loess Science, Institute of Earth Environment, Chinese
8	Academy of Sciences, Xi'an 710061, China
9	² Xi'an Institute for Innovative Earth Environment Research, Xi'an, China
10	³ National Observation and Research Station of Regional Ecological Environment Change
11	and Comprehensive Management in the Guanzhong Plain, Xi'an, China
12	
13	
14	*Corresponding author: Jianjun Li, e-mail address: lijj@ieecas.cn
15	

Abstract. This study investigated the vertical distribution of PM_{2.5} and size-segregated aerosols at the foot and top of Mount Hua in Northwest China, focusing on C2 formation and its δ^{13} C characteristics influenced by dust transport. Under non-dust conditions, PM_{2.5} and diacids concentrations at the foot were 4.5 and 2.1 times higher than those at the top, with stronger local anthropogenic signals (C₉, 5.67 times higher) and pronounced day-night differences for diacids variation. Higher C₂/C₄ (5.84 vs. 4.74), C₃/C₄ (1.04 vs. 0.56) ratios and δ¹³C values (-21.5‰ vs. -27.6‰) at the top indicated photochemical aging during aerosol transport. C₂ concentration was positively correlated with aerosol liquid water content and its size distribution pattern matched with precursors, confirming aqueous-phase oxidation as the dominant formation pathway. During dust events, PM_{2.5} concentrations at the foot and top reached 457 μg m⁻³ and 165 μg m⁻³, but C₂ concentrations in PM_{2.5} decreased by 59% (foot) and 25% (top), while δ^{13} C values of C₂ exhibited a positive shift (foot: -27.6% to -23.9%; top: -21.5% to -13.2%), attributed to alkaline dust catalyzing ¹³C-enriched oxalate formation. mGly became the second most abundant acid due to enrichment on dust-particle surfaces. Sizesegregated data revealed decreased fine-particle C₂ but increased coarse-particle C₂, elevating the coarse-to-fine particle ratio from 0.3~0.4 to 0.6~1.1. These findings offer valuable insights into the altitude-dependent transformation of SOA affected by dust transport, enhancing our understanding of mountain atmospheric chemistry and regional air quality.

- Keywords: Dicarboxylic acids, dust particles, size distribution, stable carbon isotopes (δ^{13} C),
- 35 aqueous-phase oxidation, heterogeneous reactions

16

17

18

19

20

21

22

23

24

25

26

27

28

29

30

31

32

1 Introduction

36

37 Dust cycling is crucial to Earth's climate system (Maher et al., 2010; Liang et al., 2022). Mineral particles from dust storms absorb and scatter solar radiation (Kumar et al., 2014), 38 altering regional heat balance and cloud properties, which in turn affects precipitation 39 (Mahowald et al., 2014; Kok et al., 2023; Marx et al., 2024; Xu-Yang et al., 2025). They 40 41 also act as effective ice-nucleating particles (INPs) in mixed-phase clouds, regulating ice formation and the radiation budget (Fan et al., 2016; Vergara-Temprado et al., 2018; Kawai, 42 et al., 2021; Chen et al., 2024). Dust particles often contain high levels of salts, bacteria, and 43 heavy metals, posing potential risks to human health and plant growth (Yamaguchi et al., 2016; 44 Luo et al., 2024). Dust not only impairs air quality locally but also undergoes long-range 45 transport, ultimately affecting both hemispheric and global climate systems (Pan et al., 2025). 46 During transport, mineral dust may undergo heterogeneous reactions, forming secondary 47 aerosols that aid cloud formation (Wang et al., 2020; Bikkina et al., 2023). The large surface 48 49 area of these particles facilitates reactions that alter radiation transfer and photolysis rates (Sullivan et al., 2007a). 50 Over the past 500 years, East Asia has been frequently hit by dust storms (Zhang et 51 52 al., 2021; Wu et al., 2022). The Taklimakan and Gobi Deserts, the primary sources of East 53 Asian dust, emit over 800 million tons of dust to downwind areas annually (Sullivan et al., 2007b; Wang et al., 2015; Ren et al., 2019; Zhu and Liu, 2024). Northwestern and northern 54 China, frequently experience dusty weather due to these desert emissions (Gui et al., 2022; 55 56 Liang et al., 2022). In spring 2023, Mongolia contributed over 42% of the dust concentration in northern China (Chen et al., 2023). Although dust storms are more 57 58 common in China during spring (Sun et al., 2001), a large-scale, high-intensity dust storm hit northern China on January 10, 2021. This severe dust storm, originating from southern 59 Mongolia and western Inner Mongolia, triggered rapid air quality deterioration across 60 downwind regions. Our synchronized field observations of PM_{2.5} and size-segregated aerosols 61 62 at the top of Mount Hua and on the ground in the winter of 2021 successfully captured this large-scale dust event, as shown in Fig. S1, extensively covering Northern China and the 63

Guanzhong Plain. Liu et al. (2024) compared and analyzed the concentrations and size distributions of water-soluble inorganic ions during dust and non-dust periods, finding that the impact of dust on ground aerosols in the Guanzhong Plain is weaker than that in the free troposphere. Nevertheless, the specific mechanisms through which dust affects organic components, particularly secondary organic aerosol (SOA) and their precursors in the ground and troposphere remain unclear.

To investigate these processes, this study focuses on dicarboxylic acids (diacids), which serve as key tracers for SOA (Xu et al., 2022). As important components of water-soluble organic carbon, diacids are widely distributed in the atmosphere from the surface layer to the free troposphere (Fu et al., 2008; Myriokefalitakis et al., 2011). Conventional theory suggests that aqueous-phase chemical reactions occur predominantly in submicron particles containing water or cloud droplets (Lim et al., 2010; Ervens et al., 2011; Lamkaddam et al., 2021). However, field observations have reported the coexistence of oxalate and nitrate in supermicron particles during dust events (Falkovich and Schkolnik, 2004; Sullivan et al., 2007a; Wang et al., 2015; Xu et al., 2020). To explain this, Wang et al. (2015) proposed that the reaction of nitric acid and/or nitrogen oxides with dust generates (Ca(NO₃)₂), which absorbs water vapor to form an aqueous phase on the dust surface. This enables the partitioning of gas-phase watersoluble organic precursors into this aqueous phase, followed by their further oxidation to form oxalic acid (C₂). Research by Li et al. (2025) provides direct evidence for this mechanism, showing that aqueous nitrate coatings (Ca(NO₃)₂), due to their very low deliquescence relative humidity (absorbing water at atmospheric RH > 8%), effectively promote the formation of aqueous secondary organic aerosols (aqSOA). Thus, aged dust surfaces provide critical reactive interfaces for aqSOA formation.

Tropospheric aerosols in high mountain areas are significantly influenced by long-range transport of surface pollutants, making them more representative of regional atmospheric quality. Our previous study (Shen et al., 2023) demonstrated that summer daytime valley winds on Mount Hua transport organic acids from the foot to top, thereby altering the chemical composition of the free troposphere and establishing distinct formation pathways of C₂ at

different altitudes. This study examines aerosol vertical distribution characteristics in winter. Low temperatures cause a significant reduction in the boundary layer height over Mount Hua, which inhibits the diffusion of local pollutants to the top. Consequently, the top remains in a free tropospheric environment where aerosols originate primarily from long-range transport from dust source regions (Liu et al., 2024). During the observational period, we documented a major dust event in which particles from dust source regions were directly transported to the top. There, they mixed with local anthropogenic pollutants, triggering complex atmospheric chemical reactions that resulted in notable vertical differences in aerosol chemical properties. However, the influence of heterogeneous reactions on dust aerosol surfaces on the generation of organic acids, particularly their role in modifying C₂ formation mechanisms at different altitudes remains unclear. Therefore, using observational data from a typical dust event in winter 2021, this study focuses on examining the impacts of dust transport on the molecular distribution, particle size characteristics of diacids, and the formation mechanisms of C₂. The work aims to elucidate the key role of heterogeneous chemical reactions on the surfaces of dust aerosols in the formation of SOA, providing new insights into regional atmospheric chemical processes during dust events.

2 Experimental and methods

2.1 Sample collection

Samples were collected simultaneously at the free troposphere and the ground surface during December 17, 2020 to January 12, 2021. The sampling site at the ground surface is located on Yinquan Road, Huayin City, Weinan (34°31'N, 110°04'E; ~500 m a.s.l) (referred to as "Foot"), while alpine sampling site is located at the summit of the west peak of Mount Hua (34°28'N, 110°05'E; ~2065 m a.s.l) (referred to as "Top") (Fig. 1). PM_{2.5} aerosol samples was collected using medium-flow sampler (HC-1010, China Qingdao Company, China) at a flow rate of 100 L min⁻¹ with a duration of 11 hours for each sample during the day (from 08:00 to 19:00) and night (from 20:00 to 07:00 the next day). A total of 54 samples were collected at both the alpine region and ground. The size-segregated samples were collected for ~71 h in each set using an Andersen multi-stage impactor (Andersen, Thermo electronic, USA) at a flow

- rate of 28.3 L min⁻¹ with 9 size bins as < 0.4, 0.4-0.7, 0.7-1.1, 1.1-2.1, 2.1-3.3, 3.3-4.7, 4.7-1.1
- 5.8, 5.8–9.0 and > 9.0 μ m, respectively. In a total of 9 sets of size-segregated samples were
- 122 collected. All the samples were collected onto pre-combusted (450°C for 6 h) quartz fiber filters
- produced by Whatman, UK. After sampling, the filters were stored in -18°C until analysis.
- 124 **2.2 Laboratory Analysis**

2.2.1 Determination of carbonaceous species and water-soluble inorganic ions

- The concentrations of organic carbon (OC) and elemental carbon (EC) in PM_{2.5} were
- determined using a DRI Model 2001 carbon analyzer (Atmoslytic Inc., USA), following the
- 128 IMPROVE thermal/optical reflectance (TOR) protocol (Cao et al., 2007). A 0.526 cm² filter
- punch was heated stepwise in pure helium (at 120 °C, 250 °C, 450 °C, and 550 °C) followed
- by heating in a 2% oxygen/helium atmosphere (at 550 °C, 700 °C, 800 °C). The method
- detection limits were 0.41 μ g cm⁻² for OC and 0.03 μ g cm⁻² for EC.
- Water-soluble components were extracted from a quarter of each filter using 40 mL of
- ultrapure water (Milli-Q, 18.2 MΩ, Merck, France) via a combined process of 1-hour
- ultrasonication and 1-hour mechanical shaking. After filtration through a 0.45 µm membrane,
- the extracts were preserved at 4 °C for subsequent analysis. Water-soluble inorganic ions (NH₄⁺,
- 136 K⁺, Mg²⁺, Ca²⁺, Cl⁻, NO₃⁻, and SO₄²⁻) were analyzed by ion chromatography (Metrohm 940,
- 137 Switzerland). Anions and cations were separated using an IonPac AS23 column and an IonPac
- 138 CS12A column, with 9.0 mM Na₂CO₃ and 20 mM methanesulfonic acid as eluents,
- respectively (Zhang et al., 2011). Concurrently, water-soluble organic carbon (WSOC) was
- determined using a total organic carbon (TOC) analyzer (TOC-L CPH, Shimadzu, Japan) (Li
- et al., 2019). The detection limits for inorganic ions ranged from 0.008 to 0.022 µg m⁻³, while
- those for total carbon (TC) and inorganic carbon (IC) were 0.07 mg L^{-1} and 0.08 mg L^{-1} ,
- respectively.
- Aerosol liquid water content (ALWC) was calculated using the ISORROPIA-II model
- 145 (Fountoukis and Nenes, 2007), based on the concentrations of water-soluble inorganic ions and
- meteorological parameters including relative humidity (RH) and temperature (T).
- Meteorological data for the top and the foot were obtained from the Mount Hua Meteorological

Station and the Huayin Meteorological Bureau, respectively. All statistical analyses were performed using SPSS.

2.2.2 Determination of dicarboxylic acids and related compounds

148

149

150

151

152

153

154

155

156

157

158

159

160

161

162

163

164

165

166

167

168

169

170

171

172

173

174

175

The analysis of diacids, keto-carboxylic acids, and α-dicarbonyls in PM_{2.5} and sizesegregated aerosols was conducted based on an established derivatization method (Shen et al., 2022). A quarter of each filter was extracted by ultrasonicating in ultrapure water (Milli-Q, 18.2 M Ω , Merck, France) for three sequential 15-minute intervals. To maximize the recovery of low-molecular-weight acids (e.g., C₂), the extracts were alkalized to pH 8.5–9.0 with 0.1 M KOH prior to the concentration step. The aqueous extracts were concentrated to near-dryness under vacuum in a water bath maintained at 55 °C (evaporation was halted immediately after the disappearance of the last drop of solvent). The dried residues were derivatized with 14% BF₃/n-butanol at 100°C for 1 hour to convert carboxyl groups into dibutyl esters and oxo groups into dibutoxyacetals. After the reaction, the derivatives were sequentially dissolved in n-hexane, acetonitrile, and pure water, followed by triple extraction via vortex mixing to remove watersoluble inorganic substances. The aqueous lower layer was removed using a Pasteur pipette. The n-hexane layer was concentrated by rotary evaporation and N₂ blow-down, reconstituted in 100 µL n-hexane, and finally analyzed by GC-FID (HP 6890, Agilent Technologies, USA) (Wang et al., 2012). The recovery of the target compounds was 83% for C2 and ranged from 87% to 110% for other diacids. Stable carbon isotopic compositions (δ^{13} C) of C₂ were determined using gas chromatography-isotope ratio mass spectrometry (GC-IRMS; Delta V Advantage, Thermo Fisher Scientific, Franklin, MA, USA) following established protocols (Kawamura and Watanabe, 2004). To ensure analytical precision (standard deviation < 0.2%), derivatized samples were analyzed in triplicate. Final δ^{13} C values of free oxalic acid were calculated via mass-balance correction to account for isotopic contributions from the BF₃/n-butanol derivatizing agent.

3 Results and discussion

3.1 Vertical differences in PM_{2.5} chemical composition at the foot and top of Mount Hua

during non-dust periods

176

177

178

179

180

181

182

183

184

185

186

187

188

189

190

191

192

193

194

195

196

197

198

199

200

201

202

203

During non-dust periods, significant vertical differences were observed in the chemical composition of PM_{2.5} between the foot and top of Mount Hua. The average PM_{2.5} concentration at the foot $(127 \pm 48 \ \mu g \ m^{-3})$ was 4.5 times higher than that at the top $(28 \pm 14 \ \mu g \ m^{-3})$, with a mean difference of 99 μ g m⁻³ (95% CI: 86 to 113; t (61.05) = 14.60, p < 0.001) (Supplementary Table S1 and Table S3a). Carbonaceous aerosols and water-soluble ions were significantly enriched at the foot (all p < 0.001; Table S3a). As key components of WSOC (Kawamura et al., 2016; Yang et al., 2020), the total concentration of diacids at the foot ($1808 \pm 1280 \text{ ng m}^{-3}$) was approximately 2.1 times higher than those at the top (860 \pm 534 ng m⁻³), with a mean difference of 718 ng m⁻³ (95% CI: 453 to 983; t (69.15) = 5.40, p < 0.001; Table S3b). The spatial difference was most pronounced for azelaic acid (C₉), a biomarker of biomass burning (Kalogridis et al., 2018; Shen et al., 2022), with the concentration at the foot (153 \pm 110 ng m^{-3}) being 5.7 times higher than that at the top (27 ± 18 ng m^{-3}), corresponding to a mean difference of 126 ng m⁻³ (95% CI: 95 to 156; t (54.77) = 8.24, p < 0.001; Table S3b). Consequently, the contribution of C_9 to total diacids was substantially greater at the foot (8.5%) than at the top (3.2%) (Fig. 2b). Correlation analysis of PM_{2.5} and its chemical components revealed no significant relationship between the two sites during winter, contrasting with the positive correlations observed in summer (Shen et al., 2023). Combined with ion composition and back-trajectory analysis from Liu et al. (2024), these findings indicate that pollutants at the top primarily originate from regional transport from the northwestern direction with minimal vertical mixing, while components at the foot of the mountain were mainly controlled by local emission sources. Day-night differences provide further evidence supporting this conclusion. At the foot of the mountain, PM_{2.5}, ionic components, and carbonaceous components (except for NO₃⁻ and NH_4^+) all showed significant day-night differences (p < 0.05; Table S4a). Among the diacids, methylglyoxal (mGly) exhibited the most pronounced day-night differences (daytime: $128 \pm$ 49 ng m $^{-3}$, 47% higher than nighttime: 87 ± 42 ng m $^{-3}$, p < 0.001; Fig. S2, Table S4b). As the terminal product of diacids photo-oxidation (Kawamura and Sakaguchi, 1999), C2 also

displayed marked day-night differences (daytime: 766 ± 552 ng m⁻³ vs. nighttime: 585 ± 497 ng m^{-3} , p = 0.023), reflecting strong anthropogenic influence on ground-level photochemistry. In contrast, C_2 at the top of the Mount Hua (daytime: 312 ± 224 ng m⁻³ vs. nighttime: $299 \pm$ 186 ng m⁻³; p = 0.941) and its precursors showed no clear day-night differences (p = 0.341– 0.917; Table S4c), consistent with the patterns of $PM_{2.5}$ (p = 0.979), OC (p = 0.766), and other major components (Table S4a). Such stability is a typical characteristic of high-altitude sites located above the planetary boundary layer, primarily governed by regional transport processes (Fu et al., 2008; Li et al., 2012; Meng et al., 2014), indicating that aerosol processes in the free troposphere differ from those at ground level. In this high-altitude environment, in-cloud processes represent a key pathway for aqSOA formation. Studies have shown that C₂ mainly originates from the in-cloud oxidation of precursors such as glyoxal (Gly) and isoprene (Warneck, 2003; Lim et al., 2005; Carlton et al., 2006), a mechanism supported by global model simulations (Myriokefalitakis et al., 2011). Additionally, the photochemical decomposition of C₂ following its association with Fe-containing particles in clouds (Zhang et al., 2019) also contributes to the stable distribution of organic acid concentrations at high altitudes.

Aerosol aging indicators further confirmed distinct oxidation processes between different altitudes. According to existing research, succinic acid (C₄) can be via hydroxylation to generate C₂ and malonic acid (C₃), while C₃ can be further converted to C₂ through intermediates such as hydroxymalonic acid or ketomalonic acid (Kawamura et al. 1993; Kunwar and Kawamura, 2014; Hoque et al., 2017). Therefore, the C₂/C₄ and C₃/C₄ ratios are widely used as effective indicators for assessing the extent of photochemical aging in organic aerosols (Kawamura et al., 2016; Meng et al., 2018; Shen et al., 2022). In this study, the C₂/C₄ ratio at the top of Mount Hua was 5.84 ± 0.32 , and the C₃/C₄ ratio was 1.04 ± 0.08 , both higher than the corresponding values at the foot (4.74 ± 0.28 and 0.56 ± 0.05 , respectively; Fig. 2c). These results are consistent with reports from high-altitude areas such as Mount Tai (Wang et al., 2009; Meng et al., 2018) and Mount Hua (Meng et al., 2014), collectively confirming that

the atmosphere undergoes more significant photochemical aging during long-range transport at high altitudes.

This study compared the correlations between C_2 and its key precursors at the foot and top of Mount Hua (Fig. 3a–d, 3i–l), revealing differences in atmospheric oxidation pathways across altitudes. Building on this, the synergistic effects of inorganic ions and ALWC on C_2 formation were investigated (Fig. 3e–h, 3m–p), thereby elucidating the aqueous-phase reaction mechanisms and the role of environmental factors such as humidity in C_2 generation. Results showed that C_2 exhibited the strongest correlation with glycolic acid (ωC_2) ($R^2 = 0.88$ at the foot, $R^2 = 0.95$ at the top, p < 0.01; Fig. 3 d, l). Other key precursors included Gly ($R^2 = 0.57$ -0.67, $R^2 = 0.58$ -0.81, $R^2 = 0.58$ -0.85, $R^2 = 0.58$ -0.81, $R^2 = 0.58$ -0

Contrary to previous studies (Wang et al., 2012; Meng et al., 2018), we found that C_2 correlated more strongly with NO_3^- ($R^2 = 0.79$, p < 0.01; Fig. 3f) than with SO_4^{2-} ($R^2 = 0.71$, p < 0.01; Fig. 3e) at the foot. The difference mainly stems from strong influences of local anthropogenic emissions (e.g., traffic and industrial activities) at the foot, which provide abundant NO_x and lead to an increased proportion of NO_3^- in $PM_{2.5}$. Since NO_3^- is more hygroscopic than SO_4^{2-} , its elevated concentration further enhances ALWC, thereby promoting aqSOA formation and intensifying heterogeneous reaction processes (Huang et al., 2025). In contrast, at the top of Mount Hua, C_2 exhibited a higher correlation with SO_4^{2-} ($R^2 = 0.63$, p < 0.01; Fig. 3m) than with NO_3^- ($R^2 = 0.37$, p < 0.01; Fig. 3n). This phenomenon is closely related to the active in-cloud processes in the free troposphere mentioned above. SO_4^{2-} at the top primarily originates from the oxidation of SO_2 within cloud droplets (Yermakov et al., 2023), a process dominated by heterogeneous reactions (Wang et al., 2025). Meanwhile, cloud droplets also provide key reaction media for the aqueous-phase photooxidation of C_2 precursors

such as Gly and ωC_2 (Warneck, 2003).

ALWC exhibited a humidity-dependent effect on C_2 formation. Under RH<75%, ALWC was positively correlated with C_2 concentration ($R^2 = 0.36$ -0.44, p < 0.01; Fig. 3g, 3o), reflecting the promotion of precursor dissolution and oxidation by the expansion of the aqueous phase. However, when RH exceeded 75%, supersaturation shifted the gas-particle partitioning equilibrium, causing C_2 concentrations to decrease with increasing ALWC. After excluding high-humidity data, the correlation between ALWC and C_2 significantly strengthened ($R^2 = 0.59$, p < 0.01; Fig. 3h, 3p), confirming that aqueous-phase oxidation is the primary pathway for C_2 formation during non-dust periods. This finding complements the research by Yang et al. (2022) on the synergistic effects of humidity and pH, jointly revealing the complex regulatory mechanisms of C_2 formation under different humidity conditions.

3.2 Impact of dust transport on PM_{2.5} chemical composition

On January 10, 2021, an extensive and intense dust storm, driven by successive cold fronts and sustained high-velocity winds, swept across northern China, triggering a dramatic surge in PM_{2.5} concentrations (Fig. S3). At the foot of Mount Hua, PM_{2.5} concentrations rapidly rose from 95 μ g m⁻³ to 457 μ g m⁻³ within 24 hours, reaching 3.4 times the non-dust average (127 ± 48 μ g m⁻³). Concurrently at the top, PM_{2.5} climbed from 46 to 165 μ g m⁻³, representing a 5.9-fold rise compared to typical conditions (28 ± 14 μ g m⁻³). The cleaner atmospheric environment at the top amplified the relative impact of dust transport, while at the foot, existing local pollution partially masked the dust contribution. This contrast highlights the altitude-dependent response to dust events, with the top showing greater sensitivity due to its lower background pollution levels.

HYSPLIT trajectory analysis revealed the dust originated from the Inner Mongolia-Gansu arid region and was transported along a northwest path to the study area (Fig. S4). Dust transport was closely linked to atmospheric circulation, especially in the troposphere, where changes in wind speed play a key role in dust dispersion (Yang et al., 2017). During the dust period, wind speeds at the foot increased from 2.0 to 5.3 m s⁻¹, and high-altitude wind speeds reached 12.2 m s⁻¹, higher than the average wind speed during non-dust periods (5.4 ± 3.0 m

 s^{-1}).

Although PM_{2.5} absolute concentrations rose during the dust period, component concentration changes at the two sites differed markedly. At the foot of the Mount Hua, EC concentrations remained relatively stable (4.5 ± 2.1 during non-dust vs. 4.8 ± 1.8 μg m⁻³ during dust; Table S2). OC increased from 17 ± 8.0 to 19 ± 4.6 μg m⁻³, but its mass fraction in PM_{2.5} decreased substantially from 13.4% to 4.4%, reflecting the overwhelming contribution of mineral dust. The top exhibited different characteristics, with both EC and OC concentrations doubling from 0.9 to 1.8 μg m⁻³ and 4.7 to 9.4 μg m⁻³ respectively. OC maintained a higher mass fraction of 6.5% compared to 4.4% at the foot. These patterns indicate efficient mixing of dust with anthropogenic carbonaceous aerosols during long-range transport, coupled with more vigorous secondary formation processes in the free troposphere (Wang et al., 2023; Zheng et al., 2024).

Concentrations of mineral components like calcium and magnesium ions (Ca²⁺ and Mg²⁺) rose (foot: 1.8 to 7.7 μg m⁻³; top: 0.7 to 3.2 μg m⁻³), confirming their established role as reliable

Concentrations of mineral components like calcium and magnesium ions (Ca²⁺ and Mg²⁺) rose (foot: 1.8 to 7.7 µg m⁻³; top: 0.7 to 3.2 µg m⁻³), confirming their established role as reliable tracers of dust emissions (Li et al., 2016; Liu et al., 2024). SO₄²⁻ concentrations also increased at both sites (foot: 5.8 to 10.0 µg m⁻³; top: 3.8 to 8.7 µg m⁻³). This increase can be attributed to both the release of inherent sulfate species in dust (e.g., CaSO₄) (Wu et al., 2012) and heterogeneous reactions on dust particle surfaces, where transition metals such as Fe (III) and Mn (II) catalyze the conversion of SO₂ to SO₄²⁻ (Harris et al., 2013; Myriokefalitakis et al., 2022).

Dust transport altered the concentrations and molecular distribution of diacids and their precursors. Although C_2 remained the most concentrated acidic molecule during dust periods, its absolute concentration decreased noticeably. At the foot of Mount Hua, C_2 concentrations dropped from 674 ± 528 ng m⁻³ (non-dust periods) to 276 ± 20 µg m⁻³ (dust periods), decrease by 59%. At the top of Mount Hua, C_2 concentrations decrease from 306 \pm 204 ng m⁻³ to 229 \pm 45 ng m⁻³, a reduction of 25%. Severe ozone (O₃) pollution was present in this dust storm event, and the particulate eruption promoted the generation and dispersion of O₃ pollutants. O₃ concentrations at the foot increased sharply from 15 µg m⁻³ to 62 µg m⁻³ (Fig.

S3), much higher than the non-dust average of $26 \pm 19~\mu g~m^{-3}$. The dust's extinction effect likely reduced aerosol optical thickness, enhancing surface UV radiation. Combined with a local temperature rise ($\Delta T = +5.8^{\circ}C$), this probably triggered free-radical chain reactions, promoting the heterogeneous oxidation of C_2 on mineral surfaces (Usher, et al., 2003; Lu et al., 2023). Notably, the proportion of C_2 in total diacids exhibited contrasting trends at the two sites, decreasing from 37.3% to 32.2% at the foot and increasing from 35.5% to 42.8% at the top (Fig. 4c). This divergence could be closely related to the humidity levels at the two sites. During the dust event, the lower relative humidity at the foot (RH = 24 ± 8.5%) suppressed aqueous-phase oxidation, whereas the higher humidity at the top (RH = 44 ± 11%) favored C_2 formation through such reactions. Additionally, variations in aerosol sources, transport pathways, aging processes, and potential contributions from other chemical reactions may also have influenced C_2 generation.

As a major atmospheric keto acid and key precursor of C₂ (Kawamura et al., 2012; 2013), ωC₂ ranked second among the acids detected at both sites during non-dust periods, with concentrations of 214 \pm 199 ng m⁻³ at the foot and 77 \pm 52 ng m⁻³ at the top of Mount Hua. However, during dust periods, mGly became the second most abundant acid at both sites due to its enrichment on dust-particle surfaces. At the foot, mGly concentration reached 116 ± 34 ng m⁻³ (13.6% of total diacids), up from 5.9% in non-dust periods. At the top, mGly concentration was 38 ± 9 ng m⁻³ (7.1% of total diacids) (Fig. 4b), slightly higher than the nondust 5.6%. Phthalic acid (Ph), a photo-oxidation product of naphthalene and other aromatic hydrocarbons, primarily originates from industrial processes and incomplete combustion of coal in heavy and diesel vehicles (Ho et al., 2006). At both foot and top of Mount Hua, the proportion of Ph remains relatively stable, accounting for approximately 4% during both dust and non-dust periods, indicating that its sources are stable and closely related to regional industrial activities and traffic emissions. During dust periods, the C₂/C₄ ratios at the foot and top of Mount Hua rose to 5.24 and 7.75 (Fig. 4c), showing stronger aerosol aging. However, the C₃/C₄ ratio at top of Mount Hua dropped to 0.70, this might result from the combined effects of selective adsorption of C2 onto dust particles and enhanced photolysis of C₃ on mineral dust surfaces.

3.3 Size distribution characteristics of diacids and related compounds during non-dust and dust periods

During non-dust periods, the size distribution of C₂ at both the foot and top of Mount Hua exhibited a distinct bimodal distribution (Fig. 5a and 5(a)), characterized by a primary peak in the fine particle mode (0.4-1.1 μm) and a secondary peak in the coarse particle mode (4.7-5.8 μm). Fine particles, with their greater specific surface area and hygroscopic nature, provide a conducive liquid-phase environment that enhances the oxidation of precursors such as mGly and Pyr, leading to C₂ formation (Ervens et al., 2011; Wang et al., 2015). The high correlation between C₂ and secondary inorganic ions (SO₄²⁻, NO₃⁻, NH₄⁺) (with R² values of 0.92-0.95 at the foot and 0.48-0.92 at the top, p <0.01; as shown in Fig. 6) supports this mechanism, confirming that C₂ formation during non-dust periods primarily relies on liquid-phase oxidation reactions on fine particle surfaces. The lower R² values at the top may be due to the greater influence of long-range transport at high-altitude sites, resulting in more complex sources of precursors. C₂ in the coarse particle mode likely originates from direct adsorption of biogenic emissions (such as plant waxes) or heterogeneous oxidation of gas-phase precursors on mineral dust surfaces (Wang et al., 2012).

The distribution patterns of short-chain diacids, such as C_3 and C_4 are similar to that of C_2 (Fig. 5b-c and 5(b)-(c)), with primary peaks at 0.4-1.1 µm and secondary peaks at 4.7-5.8 µm, indicating that these acids mainly come from fine particles. In contrast, glutaric (C_5) acid shows distinct distribution characteristics at the two sites. At the foot, it exhibits a unimodal distribution in the coarse particles (4.7-5.8 µm) (Fig. 5d), while at the top, it displays a bimodal distribution (0.4-1.1 µm and 4.7-5.8 µm) (Fig. 5(d)). This significant difference in modal structure suggests that different atmospheric processes govern the behavior of C_5 at different altitudes. Adipic (C_6) acid shows a bimodal distribution at both sites, probably resulting from the oxidation of cyclohexene (in the fine mode) or adsorption of gas-phase precursors on coarse particle surfaces (Deshmukh et al., 2016). Azelaic (C_9) acid is enriched only in fine particles at the foot, which may be closely related to the oxidation of unsaturated fatty acids emitted from

biomass burning in northern regions during winter (Deshmukh et al., 2016). The coarse particle fraction of Ph likely forms through gas-phase adsorption, consistent with the strong adsorption characteristics of coarse particles reported by Kanellopoulos et al. (2021).

The particle size distributions of mGly (Fig. 5g and 5(g)) and ω C₂ (Fig. 5j and 5(j)) showed remarkable consistency with that of C₂ (Fig. 5a and 5(a)), providing direct evidence that aqueous-phase oxidation serves as the predominant formation pathway for C₂. Pyr exhibited distinct altitudinal variation in its distribution characteristics. At the top of Mount Hua, Pyr displayed a similar size distribution pattern to C₂, indicating their shared photochemical origin. In contrast, at the foot, Pyr demonstrated enrichment in coarse particles (4.7-5.8 µm), likely attributable to heterogeneous reactions of gaseous precursors from local coal combustion on mineral dust surfaces. Gly also exhibits a peak in coarse particles, likely due to its strong adsorption and chemical stability on particle surfaces. The diacids concentrations are consistently lower at the top compared to the foot, which is closely tied to substantial local emissions at the lower elevation. As shown in Fig. 6, the coal combustion and biomass burning tracer Cl⁻ demonstrates an exceptionally strong correlation with C₂ (R² = 0.88, p< 0.01) at the foot.

The dust transport process impacted the size distributions of diacids in aerosols (Fig. 5). At the foot of the mountain, the C_2 concentration in fine particles (\leq 2.1 µm) decreased from 8662 ng m⁻³ to 4880 ng m⁻³ (a reduction of 43.7%) during dust events, while the concentration in coarse particle (\geq 2.1 µm) increased from 2718 ng m⁻³ to 2843 ng m⁻³ (an increase of 4.6%) (Table 3). A more pronounced change was observed at the high-altitude top of Mount Hua, where the C_2 concentration in coarse particles (2301 ng m⁻³) exceeded that in fine particles (2161 ng m⁻³) during dust events, indicating a shift in the dominant particle size distribution from fine to coarse modes. This shift in particle size distribution can be attributed to the formation of $Ca(NO_3)_2$ coatings resulting from the reaction between calcium carbonate and NO_3 ⁻ during dust aging (Li and Shao, 2009; Zhi et al., 2025). These hygroscopic coatings create favorable conditions for the adsorption and oxidation of gaseous organic compounds, thereby promoting the formation of SOA on the surfaces of coarse particles. Research by Li et al. (2025)

further confirms that aqSOA formed on dust surfaces can effectively enhance SOA production and drive a transition in the size distribution from the submicron to the supermicron range, which is highly consistent with the observational results of this study. Size-segregated ion data (Fig. S5) provide direct evidence for the above mechanism. Ca²⁺ was primarily present in the coarse mode (3.3–5.8 μm), while during dust events, NO₃⁻ at the top migrated from the fine mode (0.4–1.1 μm) to the coarse mode (3.3–5.8 μm) and coexisted with Ca²⁺ in the same size range, strongly supporting the formation of Ca(NO₃)₂ coatings on dust particle surfaces. In contrast, at the foot of the mountain, although the concentration of NO₃⁻ decreased, it remained predominantly in the fine mode. This spatial difference may stem from more thorough aging and reactions of aerosols at the top due to longer transport times. Meanwhile, the foot is influenced by local pollution, resulting in higher background NO₃⁻ concentrations and competitive reactions with components such as SO₄²⁻, which may collectively delay the distinct shift of NO₃⁻ to the coarse mode.

Analysis of the dust/non-dust concentration ratio (R_D/N) revealed R_D/N values of 0.3 and 0.6 for fine and coarse particles at the foot, respectively, while these values reached 0.4 and 1.1 at the top, indicating that dust processes have a more impact on the particle size distribution of diacids at high-altitude regions. Further investigations confirmed enrichment of C_2 precursors (mGly, Pyr, and ωC_2) in the coarse particle fraction (>2.1 μ m). Observational data from the top of Mount Hua revealed that the concentration ratio $(R_{D/N})$ of these precursors in coarse particles during dust periods reaches 0.8-1.4 during dust periods, higher than the 0.5-0.7 ratio in fine particles (\leq 2.1 μ m), demonstrating the crucial contribution of heterogeneous oxidation on dust particle surfaces to C_2 formation. Throughout dust episodes, the particle size distribution patterns of diacids (C_2 - C_6) consistently displayed a pronounced shift from fine to coarse particles (4.7-5.8 μ m) (Fig. 5). Notably, concentrations of the biomass burning tracer C_9 decreased during dust episodes, while Ph and isophthalic acid (iPh) showed distinct peaks in the coarse particle mode. This phenomenon indicates that dust particles effectively scavenge gaseous pollutants through strong adsorption, thereby suppressing the formation of local fine-mode SOA. However, these gaseous precursors adsorbed onto coarse particle surfaces can still

undergo heterogeneous oxidation reactions to form SOA.

427

428

429

430

431

432

433

434

435

436

437

438

439

440

441

442

443

444

445

446

447

448

449

450

451

452

453

454

During dust events, the correlation between C₂ and mineral ions (Ca²⁺, Mg²⁺) showed significant enhancement (with R² values of 0.33, 0.30; p<0.05 at the foot and 0.65, 0.39; p<0.01 at the top). This finding showed excellent agreement with the recent research results of Li et al. (2025), who similarly observed stronger correlations between Ca^{2+} and C_2 ($R^2 = 0.46-0.95$) in the coarse particle phase. This arises as organic acids like C₂ in aged carbonate-containing dust particles react with carbonates to form stable salts (Ervens et al., 2008; Lim et al., 2010). This process inhibits the volatility of organic acids and stabilizes them in the coarse particle phase. Furthermore, due to differences in rock types and weathering processes, Asian dust particles inherently contain higher concentrations of alkaline metal elements (Ca and Mg) compared to dust from other regions (Yu et al., 2025). The size-resolved correlations between C2, Ca2+, and Mg²⁺ (Fig. 6), further support this conclusion. During dust events, the concentrations of C₂, Ca²⁺, and Mg²⁺ exhibited synchronous increases with increasing particle size. In contrast, during non-dust periods, the peak concentration of C2 occurred in the fine particle size range, while mineral ion concentrations did not show corresponding increases. As described in Section 3.2, dust events led to reductions in C_2 concentrations in $PM_{2.5}$ (foot: 674 ± 528 ng m⁻³ during non-dust periods vs. 276 ± 20 ng m⁻³ during dust periods; top: 306 ± 204 ng m⁻³ during non-dust periods vs. 229 ± 45 ng m⁻³ during dust periods).

Overall, the transformation mechanisms of C₂ and its precursors underwent alterations during dust events, shifting from aqueous-phase oxidation dominated in fine particles during non-dust periods to heterogeneous oxidation on coarse particle surfaces as the primary pathway during dust episodes. Regional comparative analysis further revealed that atmospheric chemical processes at the mountain foot were mainly influenced by local emission sources such as coal combustion and biomass burning, whereas the summit site more clearly reflected the complex interactions between long-range dust transport and regional atmospheric processes.

3.4 Stable carbon isotopes (δ¹³C) of oxalic acid

Synchronized observations at the foot and top of Mount Hua (2060 m asl) revealed an inverse correlation between C_2 concentration and $\delta^{13}C$ values in PM_{2.5} (Fig. 7a and 7b). When

 C_2 concentration at the foot increased to 2424 ng m⁻³, its δ^{13} C value decreased to -34.5‰, while at the top, a concentration of 917 ng m⁻³ corresponded to a δ^{13} C of -24.7%. Conversely, during low concentration periods, δ^{13} C at the foot rose to -21.9% (258 ng m⁻³) and at the top to -17.2% (63 ng m⁻³). This systematic variation provides clear evidence for kinetic carbon isotope fractionation during atmospheric aqueous-phase oxidation processes. Specifically, volatile organic compounds (VOCs) and semi-volatile organic compounds (SVOCs) with lower δ^{13} C values preferentially react to form aqSOA, resulting in ¹³C-depleted products (Xu et al., 2022). Spatially, the δ^{13} C values of C₂ in PM_{2.5} at the top of Mount Hua (-28.4% to -12.8%, mean -21.5%) were higher than those at the foot (-36.2% to -14.9%, mean -27.6%). This vertical gradient primarily results from long-range transport of aerosols at high altitudes coupled with deep oxidation processes. The higher C2/C4 ratio observed at Mount Hua (5.84 vs. 4.74 at the foot) indicates more pronounced atmospheric aging characteristics. This distribution pattern originates from prolonged photochemical oxidation during long-range transport, where preferential cleavage of ¹²C-¹²C bonds (due to their lower bond energy) leads to relative ¹³C enrichment in residual C₂. In contrast, surface aerosols dominated by local fresh emissions undergo shorter oxidation periods and exhibit weaker isotope fractionation effects. Moreover, δ^{13} C can provide insights into the sources of aerosols, Pavuluri and Kawamura (2016) found that biogenic aerosols had higher mean δ^{13} C values (-15.8%) than anthropogenic sources (-19.5%). Our study shows that foot aerosols were mainly influenced by anthropogenic sources (biomass burning and coal combustion), while the top was more affected by natural sources due to richer vegetation, with long-range transport potentially weakening local isotope fractionation effects. During dust events, C₂ concentrations in PM_{2.5} showed decreasing trends, declining from

455

456

457

458

459

460

461

462

463

464

465

466

467

468

469

470

471

472

473

474

475

476

477

478

479

480

481

482

During dust events, C_2 concentrations in $PM_{2.5}$ showed decreasing trends, declining from 674 ± 528 ng m⁻³ to 276 ± 20 ng m⁻³ at the foot and from 306 ± 204 ng m⁻³ to 229 ± 45 ng m⁻³ at the top of Mount Hua. Concurrently, the $\delta^{13}C$ values of C_2 exhibited distinct positive shifts, increasing from -27.6‰ to -23.9‰ at the foot and from -21.5‰ to -13.2‰ at the top. This phenomenon reveals key chemical transformation mechanisms during dust transport: alkaline mineral surfaces promote heterogeneous catalytic oxidation of C_2 precursors, with coarse-

mode mineral components (Ca^{2+}/Mg^{2+} etc.) preferentially combining with ^{13}C -labeled C_2 to form stable compounds like calcium oxalate. This mechanism is strongly supported by observational data during dust events, both oxalic acid and Ca^{2+}/Mg^{2+} concentrations showed increases with growing particle size, while exhibiting high correlations ($R^2 = 0.30$ -0.65) during dust periods. Simultaneously, ^{12}C -enriched C_2 produced on fine particle surfaces moves to coarse particles through gas-particle conversion or coagulation, resulting in ^{13}C -enriched residues remaining in fine particles. As demonstrated by the aforementioned research findings, the concentration of oxalic acid in coarse particles showed a marked increase during dust events, with this variation being particularly pronounced at the top. These two synergistic processes collectively altered both aerosol size distribution and isotopic composition characteristics.

4. Conclusions

This study provides compelling evidence for the dual role of dust transport in modulating oxalic acid formation and isotopic composition in atmospheric aerosols. Through comprehensive analysis of PM_{2.5} and size-segregated samples, we demonstrate that dust events trigger a fundamental shift in oxalic acid production pathways from predominant aqueousphase oxidation in fine particles during non-dust periods (showing strong humidity dependence below 75% RH) to mineral heterogeneous chemistry in coarse particles during dust episodes (Fig. 8). The dust induced transformations are particularly pronounced at high-altitude sites like Mount Hua, where we observed: (1) enhanced aerosol aging indicators (C2/C4 ratio increasing to 7.75); (2) δ^{13} C enrichment (+8.3% compared to non-dust periods); and (3) preferential partitioning of C₂ to coarse-mode particles (coarse/fine particle ratio reaching 1.1). These changes result from synergistic effects of surface-catalyzed oxidation favoring ¹³C retention and metal-oxalate complexation. Conversely, surface sites exhibited stronger local anthropogenic influences, with higher C_2 concentrations (674 \pm 528 ng m⁻³) but lower δ^{13} C values (-27.6%), reflecting less processed aerosols. The identified inverse C_2 - $\delta^{13}C$ relationship and altitude-dependent response to dust transport provide new quantitative tools for evaluating aerosol aging processes and improving regional air quality models, particularly in dust-prone regions under changing climate conditions.

Data availability

- The data in this study are available at https://zenodo.org/doi/10.5281/zenodo.15788834
- 513 (Shen et al., 2025).

511

514

521

522

523

Author contributions

- Jianjun Li conceived and designed the study. Minxia Shen conducted the literature search,
- 516 performed sample and data analysis, and wrote the manuscript. Jianjun Li and Qiyuan Wang
- 517 contributed to manuscript revision. Weining Qi, Yali Liu, Yifan Zhang, Wenting Dai, Lu Li,
- Xiao Guo, Yue Cao, Yingkun Jiang, Qian Wang and Shicong Li collected particulate samples
- and supervised the experiments. All authors provided critical feedback on the manuscript and
- 520 approved the final version.

Conflict of Interest

The authors declare no conflicts of interest relevant to this study.

Acknowledgments

- This work was jointly supported by the program from National Natural Science
- Foundation of China (No. 42407156), State Key Laboratory of Loess and Quaternary Geology
- 526 (SKLLOG2307), and the Natural Science Basic Research Program of Shaanxi Province
- 527 (2025JC-YBQN-450). Jianjun Li also acknowledged the support of the Youth Innovation
- 528 Promotion Association Chinese Academy of Sciences (No. 2020407).

529 References

- 530 Bikkina, P., Bikkina, S., and Kawamura, K.: Role of aerosol liquid water content on the production of
- dicarboxylic acids in the dust-laden air masses over the Arabian Sea: Implications for heterogeneous
- 532 chemistry. Atmos. Res., 289, 106743. https://doi.org/10.1016/j.atmosres.2023.106743, 2023.
- 533 Cao, J. J., Lee, S. C., Chow, J. C., Watson, J. G., Ho, K. F., Zhang, R. J., Jin, Z. D., Shen, Z. X., Chen,
- G. C., Kang, Y. M., Zou, S. C., Zhang, L. Z., Qi, S. H., Dai, M. H., Cheng, Y. and Hu. K.: Spatial and
- seasonal distributions of carbonaceous aerosols over China, J. Geophys. Res. Atmos., 112(D22),
- 536 D22S11, https://doi.org/10.1029/2006JD008205, 2007.
- Carlton, A. G., Turpin, B. J., Lim, H. J., Altieri, K. E., and Seitzinger, S.: Link between isoprene and
- secondary organic aerosol (SOA): Pyruvic acid oxidation yields low volatility organic acids in clouds,

- Geophy. Res. Lett., 33, L06822, https://doi.org/10.1029/2005GL025374, 2006.
- 540 Chen, J. C., Xu, J. Z., Wu, Z. J., Meng, X. X. Y., Yu, Y., Ginoux, P., DeMott, P. J., Xu, R., Zhai, L. X.,
- Yan, Y. F., Zhao, C. F., Li, S. M., Zhu, T., and Hu, M.: Decreased dust particles amplify the cloud cooling
- effect by regulating cloud ice formation over the Tibetan Plateau. Sci. Adv. 10(37), eado0885.
- 543 https://doi.org/10.1126/sciadv.ado0885, 2024.
- 544 Chen, S. Y., Zhao, D., Huang, J. P., He, J. Q., Chen, Y., Chen, J. Y., Bi, H. R., Lou, G. T., Du, S. K.,
- Zhang, Y., and Yang, Fan.: Mongolia contributed more than 42% of the dust concentrations in Northern
- 546 China in March and April 2023. Adv. Atmos. Sci., 40(9), 1549–1557. https://doi.org/10.1007/s00376-
- 547 023-3062-1, 2023.
- Deshmukh, D. K., Kawamura, K., and Deb, M. K.: Dicarboxylic acids, ω-oxocarboxylic acids, α-
- 549 dicarbonyls, WSOC, OC, EC, and inorganic ions in wintertime size-segregated aerosols from central
- 550 India: Sources and formation processes. Chemosphere, 161, 27–42.
- 551 <u>https://doi.org/10.1016/j.chemosphere.2016.06.107</u>, 2016.
- Deshmukh, D. K., Kawamura, K., Deb, M. K., and Boreddy, S. K. R.: Sources and formation processes
- of water-soluble dicarboxylic acids, ω-oxocarboxylic acids, α-dicarbonyls, and major ions in summer
- aerosols from eastern central India. J. Geophys. Res. Atmos., 122(6), 3630-3652.
- 555 <u>https://doi.org/10.1002/2016JD026246</u>, 2017.
- 556 Du, W., Ding, Z. J., Lei, Y. L., Zhang, S., Wu, C., Zhang, F., Wang, F. L., Lv, S. J., Liu, X. D., Meng, J.
- 557 J., and Wang, G. H.: Atmospheric fine particulate dicarboxylic acids and related SOA in winter at the
- background site of Yangtze River Delta: Implication for the long-distance transport of solid fuels
- burning. Atmos. Environ. 289, 11932. https://doi.org/10.1016/j.atmosenv.2022.119320, 2022.
- 560 Ervens, B., Turpin, B. J., and Weber, R. J.: Secondary organic aerosol formation in cloud droplets and
- aqueous particles (aqSOA): a review of laboratory, field and model studies. Atmos. Chem. Phys., 11(21),
- 562 11069–11102. https://doi.org/10.5194/acp-11-11069-2011, 2011.
- 563 Falkovich, A. H., and Schkolnik, G.: Adsorption of organic compounds pertinent to urban
- 564 environmentsonto mineral dust particles. J. Geophys. Res. Atmos., 109, D02208.
- 565 https://doi.org/10.1029/2003JD003919, 2004.
- Fan, J. Y., Wang, Y., Rosenfeld, D., and Liu, X. H.: Review of aerosol-cloud interactions: Mechanisms,

- significance, and challenges. J. Atmos. Sci., 73(11), 4221–4252. https://doi.org/10.1175/JAS-D-16-
- 568 <u>0037.1</u>, 2016.
- Fountoukis, C., and Nenes, A.: ISORROPIA II: a computationally efficient thermodynamic equilibrium
- model for K⁺-Ca²⁺-Mg²⁺-NH4⁺-Na⁺-SO₄²⁻-NO₃-Cl⁻-H₂O aerosols. Atmos. Chem. Phys., 7(17), 4639–
- 571 4659. https://doi.org/10.5194/acp-7-4639-2007, 2007.
- 572 Fu, P. Q., Kawamura K., Kanaya, Y., and Wang, Z. F.: Contributions of biogenic volatile organic
- 573 compounds to the formation of secondary organic aerosols over Mt. Tai, Central East China. Atmos.
- 574 Environ., 44, 4817–4826. https://doi.org/10.1016/j.atmosenv.2010.08.040, 2010.
- 575 Fu, T. M., Jacob, D. J., Wittrock, F., Burrows, J. P., Vrekoussis, M., and Henze, D. K.: Global budgets
- of atmospheric glyoxal and methylglyoxal, and implications for formation of secondary organic
- 577 aerosols. J. Geophys. Res. 113. D15303, https://doi.org/15310.11029/12007JD009505, 2008.
- 578 Gui, K., Yao, W. R., Che, H. Z., An, L.C., Zheng, Y., Li, L., Zhao, H. J., Zhang, L., Zhong, J. T., Wang,
- Y. Q., and Zhang, X.Y.: Record-breaking dust loading during two mega dust storm events over northern
- 580 China in March 2021: aerosol optical and radiative properties and meteorological drivers. Atmos. Chem.
- 581 Phys. 22(12), 7905–7932. https://doi.org/10.5194/acp-22-7905-2022, 2022.
- Harris, E., Bärbel Sinha, van Pinxteren, D., Tilgner, Andreas., Fomba, K. W., Schneider, J., Roth, A.,
- 583 Gnauk, T., Fahlbusch, B., Mertes, S., Lee, T., Collett, J., Foley, S., Borrmann, S., Hoppe, P., and
- Herrmann, H.: Enhanced role of transition metal ion catalysis during in-cloud oxidation of SO₂. Science,
- 585 340(6133),727–730. https://doi.org/10.1126/science.123091, 2023.
- 586 Huang, R. J., Li, Y. J., Chen, Q., Zhang, Y. L., Lin, C. S., Chan, C. K., Yu, J. Z., Gouw, J., Tong, S. R.,
- Jiang, J. K., Wang, W. G., Ding, X., Wang, X. M., Ge, M. F., Zhou, W. J., Worsnop, D., Boy, M., Bilde,
- 588 M., Dusek, U., Carlton, A. G., Hoffmann, T., McNeill, V. F., and Glasius M.: Secondary organic aerosol
- 589 in urban China: A distinct chemical regime for air pollution studies, Science, 389, eadq2840.
- 590 https://doi.org/ 10.1126/science.adq2840, 2025.
- Ho, K. F., Lee, S. C., Cao, J. J., Kawamura, K., Watanabe, T., Cheng, Y., and Chow, J. C.: Dicarboxylic
- 592 acids, ketocarboxylic acids and dicarbonyls in the urban roadside area of Hong Kong, Atmos. Environ.,
- 593 40, 3030–3040, https://doi.org/10.1016/j.atmosenv.2005.11.069, 2006.
- Hoque, M. M., Kawamura, K., and Uematsu, M.: Spatio temporal distributions of dicarboxylic acids,
- ω-oxocarboxylic acids, pyruvic acid, α-dicarbonyls and fatty acids in the marine aerosols from the North

- and South Pacific, Atmos. Res., 185, 158–168, https://doi.org/10.1016/j.atmosres.2016.10.022, 2017.
- Kalogridis, A. C., Popovicheva, O. B., Engling, G., Diapouli, E., Kawamura, K., Tachibana, E., Ono,
- 598 K., Kozlov, V. S., and Eleftheriadis. K.: Smoke aerosol chemistry and aging of Siberian biomass burning
- 599 emissions in a large aerosol chamber. Atmos. Environ. 185, 15–28.
- 600 https://doi.org/10.1016/j.atmosenv.2018.04.033, 2018.
- Kanellopoulos, P. G., Chrysochou, E., Koukoulakis, K., and Bakeas E.: Secondary organic aerosol
- markers and related polar organic compounds in summer aerosols from a sub-urban site in Athens: Size
- 603 distributions, diurnal trends and source apportionment. Atmos. Pollut. Res., 12, 1–13.
- 604 https://doi.org/10.1016/j.apr.2021.02.01, 2021.
- Kawai, K., Matsui, H., and Tobo, Y.: High potential of Asian dust to act as ice nucleating particles in
- mixed-phase clouds simulated with a global aerosol-climate model. J. Geophys. Res. Atmos., 126(12),
- 607 e2020JD034263. https://doi.org/10.1029/2020JD034263, 2021.
- Kawamura, K., and Bikkina, S.: A review of dicarboxylic acids and related compounds in atmospheric
- aerosols: Molecular distributions, sources and transformation. Atmos. Res., 170(15), 140-160.
- 610 https://doi.org/10.1016/j.atmosres.2015.11.018, 2016.
- Kawamura, K., and Ikushima, K.: Seasonal changes in the distribution of dicarboxylic acids in the urban
- atmosphere, Environ. Sci. Technol., 27, 2227-2235, https://doi.org/10.1021/es00047a033, 1993.
- 613 Kawamura, K. and Sakaguchi, F.: Molecular distributions of water soluble dicarboxylic acids in marine
- aerosols over the Pacific Ocean including tropics, J. Geophys. Res.-Atmos., 104, 3501-3509,
- 615 https://doi.org/10.1029/1998JD100041, 1999.
- Kawamura, K., and Watanabe, T.: Determination of stable carbon isotopic compositions of low
- 617 molecular weight dicarboxylic acids and ketocarboxylic acids in atmospheric aerosol and snow samples.
- 618 Anal. Chem., 76(19), 5762–5768. https://doi.org/10.1021/ac049491m, 2004.
- Kawamura, K., Ono, K., Tachibana, E., Charriére, B., and Sempéré, R.: Distributions of low molecular
- weight dicarboxylic acids, ketoacids and α -dicarbonyls in the marine aerosols collected over the Arctic
- Ocean during late summer, Biogeosciences, 9, 4725–4737, https://doi.org/10.5194/bg-9-4725-2012,
- 622 2012.
- Kawamura, K., Tachibana, E., Okuzawa, K., Aggarwal, S. G., Kanaya, Y., and Wang, Z. F.: High

- 624 abundances of water-soluble dicarboxylic acids, ketocarboxylic acids and α-dicarbonyls in the
- 625 mountaintop aerosols over the North China Plain during wheat burning season, Atmos. Chem. Phys.,
- 626 13, 8285–8302, https://doi.org/10.5194/acp-13-8285-2013, 2013.
- Kok, J. F., Storelvmo, T., Karydis, V. A., Adebiyi, A. A., Mahowald, N. M., Evan, A.T., He, C. L., and
- 628 Leung, D. M.: Mineral dust aerosol impacts on global climate and climate change. Nat. Rev. Earth Env.,
- 629 4, 71–86, https://doi.org/10.1038/s43017-022-00379-5, 2023.
- Kumar, R., Barth, M. C., Madronich, S., Naja, M., Carmichael, G. R., Pfister, G. G., Knote, C., Brasseur,
- 631 G. P., Ojha, N. and Sarangi, T.: Effects of dust aerosols on tropospheric chemistry during a typical pre-
- monsoon season dust storm in northern India. Atmos. Chem. Phys., 14, 6813-6834, 2014,
- 633 <u>https://doi.org/10.5194/acp-14-6813-2014</u>, 2014.
- 634 Kunwar, B. and Kawamura, K.: Seasonal distributions and sources of low molecular weight
- dicarboxylic acids, v-oxocarboxylic acids, pyruvic acid, a-dicarbonyls and fatty acids in ambient
- 636 aerosols from subtropical Okinawa in the western Pacific Rim, Environ. Chem., 11, 673-689,
- 637 <u>https://doi.org/10.1071/EN14097</u>, 2014.
- Lamkaddam, H., Dommen, J., Ranjithkumar, A., Gordon, H., Wehrle, G., Krechmer, J., Majluf, F.,
- 639 Salionov, D., Schmale, J., Bjelić, S., Carslaw, K. S., Haddad, I. E., and Baltensperger, U.: Large
- 640 contribution to secondary organic aerosolfrom isoprene cloud chemistry. Sci. Adv., 7, eabe2952.
- 641 https://doi.org/10.1126/sciadv.abe2952, 2021.
- 642 Li, J. J., Wang, G. H., Ren, Y. Q., Wang, J. Y., Wu, C., Han, Y., Zhang, L., Cheng, C. L., and Meng, J.
- 643 J.: Identification of chemical compositions and sources of atmospheric aerosols in Xi'an, inland China
- 644 during two types of haze events. Sci. Total Environ., 566-567, 230-237.
- 645 https://doi.org/10.1016/j.scitotenv.2016.05.057, 2016.
- 646 Li, J. J., Wang, G. H., Zhang, Q., Li, J., Wu, C., Jiang, W. Q., Zhu, T., and Zeng, L. M.: Molecular
- characteristics and diurnal variations of organic aerosols at a rural site in the North China Plain with
- implications for the influence of regional biomass burning. Atmos. Chem. Phys., 19(16), 10481–10496,
- 649 https://doi.org/10.5194/acp-19-10481-2019, 2019.
- 650 Li, J. J., Wang, G. H., Zhou, B. H., Cheng, C. L., Cao, J. J., Shen, Z. X., and An, Z. S.: Airborne
- particulate organics at the summit (2060 m, a.s.l.) of Mt. Hua in central China during winter:

- 652 Implications for biofuel and coal combustion. Atmos. Res., 106, 108–119,
- 653 https://doi.org/10.1016/j.atmosres.2011.11.012, 2012.
- 654 Li, W. J., and Shao L. Y.: Observation of nitrate coatings on atmospheric mineral dust particles. Atmos.
- 655 Chem. Phys., 9(6), 1863–1871. https://doi.org/10.5194/acp-10-10521-2010, 2009.
- 656 Li, W. J., Ito, A., Wang, G. C., Zhi, M. K., Xu, L., Yuan, Q., Zhang, J., Liu, L., Wu, F., Laskin, A., Zhang,
- D. Z., Zhang, X.Y., Zhu, T., Chen, J. M., Mihalopoulos, N., Bougiatioti, A., Kanakidou, M., Wang, G.
- H., Hu, H. L., Zhao, Y., and Shi, Z. B.: Aqueous-phase secondary organic aerosol formation on mineral
- dust, Natl. Sci. Rev., nwaf221, https://doi.org/10.1093/nsr/nwaf221, 2025.
- 660 Liang, P., Chen, B., Yang, X. P., Liu, Q. Q., Li, A. R., Mackenzie, L., and Zhang, D. G.: Revealing the
- dust transport processes of the 2021 mega dust storm event in northern China. Sci. Bull., 67(1), 21–24.
- 662 <u>https://doi.org/10.1016/j.scib.2021.08.014, 2022.</u>
- 663 Lim, H. J., Carlton, A. G., and Turpin, B. J.: Isoprene forms secondary organic aerosol through cloud
- 664 processing: model simulations. Environ. Sci. Technol. 39(12), 4441–4446.
- 665 https://doi.org/10.1021/es048039h, 2005.
- 666 Lim, Y. B., Tan, Y., Perri, M. J., S. P. Seitzinger., and Turpin., B. J.: Aqueous chemistry and its role in
- secondary organic aerosol (SOA) formation. Atmos. Chem. Phys., 10(21), 10521-10539.
- 668 https://doi.org/10.5194/acp-10-10521-2010, 2010.
- 669 Liu, H. J., Feng, Q., Huang, Y., Wu, F., Liu, Y. L., Shen, M. X., Guo, X., Dai, W. T., Qi, W. N., Zhang,
- Y. F., Li, L., Wang, Q. Y., Zhou, B. H., and Li, J. J.: Composition and size distribution of wintertime
- 671 inorganic aerosols at ground and alpine regions of northwest China. Chin. Chem. Lett., 35(11), 109636.
- 672 https://doi.org/10.1016/j.cclet.2024.109636, 2024.
- 673 Lu, Da., Li, H., Tian, M. K., Wang, G. C., Qin, X. F., Zhao, N., Huo, J. T., Yang, F., Lin, Y. F., Chen, J.,
- 674 Fu, Q. Y., Duan, Y. S., Dong, X.Y., Deng, C. R., Abdullaev, S. F., and Huang, K.: Secondary aerosol
- 675 formation during a special dust transport event: impacts from unusually enhanced ozone and dust
- backflows over the ocean. Atmos. Chem. Phys., 23(21), 13853–13868, https://doi.org/10.5194/acp-23-23
- 677 13853-2023, 2023.
- 678 Luo, Y. Y., Yao, Q., Ding, P., Hou, M., Deng, F. C., Wang, Y. B., Ding, C., Li, X., Wang, D. C., Sun, Z.
- 679 k., Tang, S., Mao, Y. X., and Yao, X. Y.: Health impacts of an extreme dust event: a case and risk

- assessment study on airborne bacteria in Beijing, China. Environ. Sci. Eur., 36:41.
- 681 <u>https://doi.org/10.1186/s12302-024-00858-0, 2024.</u>
- Maher, B. A., Prospero, J. M., Mackie, D., Gaiero, D., Hesse P. P., and Balkanski Y.: Global connections
- between aeolian dust, climate and ocean biogeochemistry at the present day and at the last glacial
- 684 maximum. Earth Sci. Rev., 99(1–2), 61–97. https://doi.org/10.1016/j.earscirev.2009.12.001, 2010.
- Mahowald, N., Albani, S., Kok, J. F., Engelstaeder, S., Scanza, R., Ward, D. S., and Flanner, M. G.: The
- size distribution of desert dust aerosols and its impact on the Earth system. Aeolian Res., 15, 53–71,
- 687 <u>https://doi.org/10.1016/j.aeolia.2013.09.002</u>, 2014.
- Marx, S. K., Hooper, J., Irino, T., Stromsoe, N., Saunders, K. M., Seki, O., Dosseto, A., Johansen, A.,
- Hua, Q., Dux, F., Jacobsen, G., and Zawadzki, A.: Atmospheric particulates over the northwestern
- Pacific during the late Holocene: Volcanism, dust, and human perturbation. Sci. Adv. 10(43), eadn3311,
- 691 https://doi.org/10.1126/sciadv.adn3311, 2024.
- 692 Meng, J. J., Wang, G. H., Li, J. J., Cheng, C. L., Ren, Y. Q., Huang, Y., Cheng, Y. B., Cao, J. J., and
- Zhang, T.: Seasonal characteristics of oxalic acid and related SOA in the free troposphere of Mt. Hua,
- 694 central China: Implications for sources and for mation mechanisms, Sci. Total Environ., 493, 1088–
- 695 1097, https://doi.org/10.1016/j.scitotenv.2014.04.086, 2014.
- 696 Meng, J. J., Wang, G. H., Hou, Z. F, Liu, X. D, Wei, B. J, Wu, C., Cao, C., Wang, J. Y., Li, J. J., Cao, J.
- 697 J., Zhang, E., Dong, J., Liu, J. Z, Ge, S. S., and Xie, Y. N.: Molecular distribution and stable carbon
- 698 isotopic compositions of dicarboxylic acids and related SOA from biogenic sources in the summertime
- atmosphere of Mt. Tai in the North China Plain, Atmos. Chem. Phys., 18, 15069-15086,
- 700 https://doi.org/10.5194/acp-18-15069-2018, 2018.
- 701 Myriokefalitakis, S., Tsigaridis, K., Mihalopoulos, N., Sciare, J., Nenes, A., Kawamura, K., Segers, A.,
- and Kanakidou, M.: In-cloud oxalate formation in the global troposphere: a 3-D modeling study. Atmos.
- 703 Chem. Phys., 11(12), 5761–5782. https://doi.org/10.5194/acp-11-5761-2011, 2011.
- 704 Myriokefalitakis, S., Bergas-Massó, E., Gonçalves-Ageitos, M., García-Pando, C. P., Noije, T., Sager,
- P. L., Ito, A., Athanasopoulou, E., Nenes, A., Kanakidou, M., Krol, M. C., and Gerasopoulos, E.:
- Multiphase processes in the EC-Earth model and their relevance to the atmospheric oxalate, sulfate, and
- 707 iron cycles. Geosci. Model Dev., 15(7), 3079–3120, https://doi.org/10.5194/gmd-15-3079-2022, 2022.

- Pan, H. Z., Hu, Z. Y., Feng, T. C., Huang, Z. W., Liu, Q. T., and Feng, G. L.: Distribution characteristics
- and air-quality effect of intercontinental transport dust: An unexpected dust storm case study in China.
- 710 Atmos. Environ., 350, 121177. https://doi.org/10.1016/j.atmosenv.2025.121177, 2025.
- Pavuluri, C. M. and Kawamura, K.: Enrichment of ¹³C in diacids and related compounds during
- 712 photochemical processing of aqueous aerosols: New proxy for organic aerosols aging, Sci. Rep., 6,
- 713 36467, https://doi.org/10.1038/srep36467, 2016.
- 714 Ren, Y. Q., Wang, G. H., Li, J. J., Wu, C., Cao, C., Li, J., Wang, J. Y., Ge, S. S., Xie, Y. N., Li, X. R.,
- 715 Meng, F. and Li, H.: Evolution of aerosol chemistry in Xi'an during the spring dust storm periods:
- 716 Implications for heterogeneous formation of secondary organic aerosols on the dust surface.
- 717 Chemosphere, 215, 413–421. https://doi.org/10.1016/j.chemosphere.2018.10.064, 2019.
- 718 Shen, M. X., Qi, W. N., Guo, X., Dai, W. T., Wang, Q. Y., Liu, Y. L., Zhang, Y. F., Cao, Y., Chen, Y. K.,
- 719 Li, L., Liu, H. J., Cao, J. J., and Li J. J.: Influence of vertical transport on chemical evolution of
- 720 dicarboxylic acids and related secondary organic aerosol from surface emission to the top of Mount
- 721 Hua, Northwest China. Sci. Total Environ., 858, 159892,
- 722 <u>http://dx.doi.org/10.1016/j.scitotenv.2022.159892</u>, 2023.
- 723 Shen, M. X., Ho, K. F., Dai, W. T., Liu, S. X., Zhang, T., Wang, Q. Y., Meng, J. J., Chow, J. C., Watson,
- J. G., Cao, J. J., and Li. J. J.: Distribution and stable carbon isotopic composition of dicarboxylic acids,
- 725 ketocarboxylic acids and α-dicarbonyls in fresh and aged biomass burning aerosols. Atmos. Chem.
- 726 Phys., 22(11), 7489–7504, https://doi.org/10.5194/acp-22-7489-2022, 2022.
- 727 Shen, M. X., Qi, W. N., Liu, Y. L., Zhang, Y. F., Dai, W. T., Li, L., Guo, X., Cao, Y., Jiang, Y. K., Wang,
- Q., Li, S. C., Wang, Q. Y., and Li, J. J: Measurement report: Observational insights into the impact of
- dust transport on atmospheric dicarboxylic acids in ground region and free troposphere. Zenodo [data
- 730 set], https://zenodo.org/doi/10.5281/zenodo.15788834, 2025.
- 731 Sullivan, R. C., and Prather, Kimberly A. Investigations of the diurnal cycle and mixing state of oxalic
- acid in individual particles in Asian aerosol outflow. Environ. Sci. Technol. 41(23), 8062-8069,
- 733 https://doi.org/10.1021/es071134g, 2007a.
- Sullivan, R. C., Guazzotti 1, S. A., Sodeman, D. A., and K. A. Prather.: Direct observations of the
- 735 atmospheric processing of Asian mineral dust. Atmos. Chem. Phys., 7(5), 1213-1236,

- 736 https://doi.org/10.5194/acp-7-1213-2007, 2007b.
- 737 Sun, J. M., Zhang, M. Y., and Liu, T. S.: Spatial and temporal characteristics of dust storms in China
- and its surrounding regions, 1960-1999: Relations to source area and climate. J. Geophys. Res.,
- 739 106(D10), 10,325–10,333, https://doi.org/10.1029/2000JD900665, 2001.
- 740 Usher C. R., Michel, A. E. and Vicki H.: Grassian Reactions on Mineral Dust Chem. Rev. 103(12),
- 741 4883–4939. https://doi.org/10.1021/cr020657y, 2003.
- Vergara-Temprado, J., Miltenberger, A. K., Furtado, K., Grosvenor, D. P., Shipway, B. J., Hill, A. A.,
- Wilkinson, J. M., Field, P. R., Murray, B. J., and Carslaw, K. S.: Strong control of southern ocean cloud
- reflectivity by ice-nucleating particles. Proc. Natl. Acad. Sci. U.S.A 115(11), 2687–2692.
- 745 https://doi.org/10.1073/pnas.1721627115, 2018.
- Wang, G. H., Kawamura, K., Cheng, C. L., Li, J. J., Cao, J. J., Zhang, R. J., Zhang, T., Liu, S. X., and
- 747 Zhao, Z. Z.: Molecular distribution and stable carbon isotopic composition of dicarboxylic acids,
- ketocarboxylic acids, and α -dicarbonyls in size-resolved atmospheric particles from Xi'an city, China.
- 749 Environ. Sci. Technol., 46(9), 4783–4791. https://doi.org/10.1021/es204322c, 2012.
- Wang, G. H., Kawamura, K., Umemoto, N., Xie, M. J, Hu, S. Y., and Wang, Z. F.: Water-soluble organic
- 751 compounds in PM_{2.5} and size-segregated aerosols over Mount Tai in North China Plain. J. Geophys.
- 752 Res. 114, 1–10. https://doi.org/10.1029/2008jd011390. D19208, 2009.
- Wang, G. H., Cheng, C. L., Meng, J. J., Huang, Y., Li, J.J. and Ren, Y. Q.: Field observation on
- 754 secondary organic aerosols during Asian dust storm periods: Formation mechanism of oxalic acid and
- 755 related compounds on dust surface. Atmos. Environ., 113, 169–176.
- 756 <u>https://doi.org/10.1016/j.atmosenv.2015.05.013</u>, 2015.
- 757 Wang, G. H., Zhang, S., Wu, C., Zhu, T., Xu, X. B., Ge, S. S., Sun, H. T., Sun Z. R., Wang, J. X., Ji,
- Y. M., Gao, J., Ren, Y. Q., Li, H., Zhang, F., Wang, Y., and Seinfeld, J. H.: Atmospheric sulfate
- 759 aerosol formation enhanced by interfacial anions. PNAS Nexus, 4, pgaf058.
- 760 <u>https://doi.org/10.1093/pnasnexus/pgaf058</u>, 2025.
- Wang, Y. D., Zhou, L., Wang, W. G., and Ge, M. F.: Heterogeneous uptake of formic acid and acetic
- 762 acid on mineral dust and coal fly ash. ACS Earth Space Chem. 4(2), 202-210,
- 763 <u>https://dx.doi.org/10.1021/acsearthspacechem.9b00263</u>, 2020.

- 764 Wang, Z., Shi, C., Zhang, H., Chen, Y. J., Chi, X. Y., Xia, C., Wang, S. Y., Zhu, Y. Z., Zhang, K., Chen,
- X. T., Xing, C., and Liu. C.: Measurement report: Dust and anthropogenic aerosols' vertical distributions
- over northern China dense aerosols gathered at the top of the mixing layer. Atmos. Chem. Phys., 23,
- 767 14271–14292, https://doi.org/10.5194/acp-23-14271-2023, 2023.
- Warneck, P.: In-cloud chemistry opens pathway to the formation of oxalic acid in the marine atmosphere.
- 769 Atmos. Environ. 37(17), 2423–2427, https://doi.org/10.1016/S1352-2310(03)00136-5, 2003.
- Wu, C. L., Lin, Z. H., Shao, Y. P., Liu, X. H., and Li, Y.: Drivers of recent decline in dust activity over
- 771 East Asia, Nat. Commun., 13, 7105. https://doi.org/10.1038/s41467-022-34823-3, 2022.
- Wu, F., Zhang, D. Z., Cao, J. J., Xu, H. M., and An, Z. S.: Soil-derived sulfate in atmospheric dust
- particles at Taklimakan desert, Geophys. Res. Lett., 39(24), L24803,
- 774 <u>https://doi.org/10.1029/2012GL054406</u>, 2012.
- 775 Xu, B. Q., Zhang, G., Gustafsson, Ö., Kawamura, K., Li, J., Andersson, A., Bikkina, S., Kunwar, B.,
- Pokhrel, A., Zhong, G. C., Zhao, S. Z., Li, J., Huang, C., Cheng, Z. N., Zhu, S. Y., Peng, P.A., and Sheng,
- 777 G.Y.: Large contribution of fossil-derived components to aqueous secondary organic aerosols in China.
- 778 Nat. Commun. 13, 5115. https://doi.org/10.1038/s41467-022-32863-3, 2022.
- 779 Xu, W. Y., Kuang, Y., Liang, L. L., He, Y., Cheng, H. B., Bian, Y. X., Tao, J. C., Zhang, G., Zhao, P. S.,
- 780 Ma, N., Zhao, H. R., Zhou, G. S., Su, H., Cheng, Y. F., Xu, X. B., Shao, M., amd Sun, Y. L.: Dust-
- dominated coarse particles as a medium for rapid secondary organic and inorganic aerosol formation in
- 782 highly polluted air. Environ. Sci. Technol., 54(24):15710–15721.
- 783 https://doi.org/10.1021/acs.est.0c07243, 2020.
- 784 Xu-Yang, Y. J. J., Skonieczny, C., Ayrault, S., Barbier, J., Bizeul, R., Bryskere, O., Chaboche, P.,
- 785 Chalaux-Clergue, T., Corcho-Alvarado, J.A., Foucher, A., Karsenti, A., Leblanc, M., Orizaola, G.,
- 786 Plautre, A., Röllin, S., Taraconat, N., Tenaud, N., Valdés, A. E., Dulac, F., and Evrard, O.: Radioactive
- 787 contamination transported to Western Europe with Saharan dust. Sci. Adv., 11(5), eadr9192.
- 788 <u>https://doi.org/10.1126/sciadv.adr9192</u>, 2025.
- Yang, C., Zhou, S. X., Zhang, C. Y., Yu, M. Y., Cao, F., and Zhang, Y. L.: Atmospheric chemistry of
- oxalate: Insight into the role of relative humidity and aerosol acidity from high-resolution observation.
- 791 J. Geophys. Res. Atmos., 127(4), e2021JD035364. https://doi.org/10.1029/2021JD035364, 2022.

- 792 Yang, J., Zhao, W. Y., Wei, L. F., Zhang, Q., Zhao, Y., Hu, W., Wu, L. B., Li, X. D., Pavuluri, C. M.,
- Pan, X. L., Sun, Y. L., Wang, Z. F., Liu, C. Q., Kawamura, K., and Fu, P. Q.: Molecular and spatial
- distributions of dicarboxylic acids, oxocarboxylic acids, and-dicarbonyls in marine aerosols from the
- 795 South China Sea to the eastern Indian Ocean, Atmos. Chem. Phys., 20(11), 6841-6860,
- 796 https://doi.org/10.5194/acp-20-6841-2020, 2020.
- 797 Yamaguchi, N., Baba, T., Ichijo, T., Himezawa, Y., Enoki, K., Saraya, M., Li, P., and Nasu, M.:
- Abundance and community structure of bacteria on Asian dust particles collected in Beijing, China,
- during the Asian Dust Season. Biol. Pharm. Bull., 39(1):68–77. https://doi.org/10.1248/bpb.b15-00573,
- 800 2016.
- Yang, Y., Russell, L. M., Lou, S. J., Liao, H., Guo, J. P., Liu, Y., Singh, B., and Ghan, S. J.: Dust-wind
- 802 interactions can intensify aerosol pollution over eastern China. Nat. Commun., 8:15333.
- 803 <u>https://doi.org/10.1038/ncomms15333</u>, 2017.
- Yermakov, A. N., Aloyan, A. E., Arutyunyan, V. O., and Pronchev, G. B.: On the mechanism of sulfur
- 805 dioxide oxidation in cloud drops. Izv. Atmos. Oceanic Phys., 59(5), 538-547.
- 806 <u>https://doi.org/10.1134/S0001433823050055</u>, 2023.
- Yu, Z. C., Song, R. Y., Wang, Q. H., Quan, J. Y., Zhang, H. Y., Fu, J. J., and Jiang, G. B.: Research
- progress of atmospheric chemical process of airborne dust particles. Environ. Chem., 44(3): 854–867.
- 809 https://doi.org/10.7524/j.issn.0254-6108.2024051303, 2025.
- 810 Zhang, G. H., Lin, Q. H., Peng, L., Yang, Y. X., Jiang, F., Liu, F. X., Song, W., Chen, D. H., Cai, Z., Bi,
- X. H., Miller, M., Tang, M. J., Huang, W. L., Wang, X. M., Peng, P. A., and Sheng, G. Y.: Oxalate
- formation enhanced by Fe-containing particles and environmental implications. Environ. Sci. Technol.,
- 53(3):1269–1277. https://doi.org/10.1021/acs.est.8b05280, 2019.
- Zhang, R. F., Gen, M. S., Liang, Z. C., Li, Y. J., and Chan, C. K.: Photochemical reactions of glyoxal
- during particulate ammonium nitrate photolysis: brown carbon formation, enhanced glyoxal decay, and
- 816 organic phase formation. Environ. Sci. Technol., 56(3), 1605–1614.
- 817 https://doi.org/10.1021/acs.est.1c07211, 2022.
- Zhang, S., Xu, H., Lan, J. H., Goldsmith, Y., Torfstein, A., Zhang, G. L., Zhang, J., Song, Y. P., Zhou,
- K., Tan, L.C., Xu, S., Xu, X. M., and Enzel, Y.: Dust storms in northern China during the last 500 years.

- 820 Sci. China Earth Sci., 64(5), 813–824. https://doi.org/10.1007/s11430-020-9730-2, 2021.
- 821 Zhu, Q. Z., and Liu, Y. J.: The dominant factor in extreme dust events over the Gobi Desert is shifting
- from extreme winds to extreme droughts. Npj clim. Atmos. Sci., 7:141, https://doi.org/10.1038/s41612-
- 823 <u>024-00689-z</u>, 2024.
- 824 Zhang, T., Cao, J. J., Tie, X. X., Shen, Z. X., Liu, S. X., Ding, H., Han, Y. M., Wang, G. H., Ho, K. F.,
- Qiang, J., and Li, W. T.: Water-soluble ions in atmospheric aerosols measured in Xi'an, China: Seasonal
- 826 variations and sources. Atmos. Res., 102(1–2), 110–119.
- 827 https://doi.org/10.1016/j.atmosres.2011.06.014, 2011.
- 828 Zheng, F. X., Li, J. W., Hua, C. J., Xie, J. L., Zhang, Y. S., Li, L.Y., Shen, S. N., Hakala, S., Yan, C.,
- Feng, Z. M., Fan, X. L., Bianchi, F., Petäjä, T., Kerminen, V., Kulmala, M., Xia, M., Zha, Q., Du, W.,
- Daellenbach, K. R., Cai, J., and Liu, Y. C.: Dust event identification and characterization with one-year
- 831 online observations in Beijing. Sci. Total Environ., 956(15), 177296.
- 832 https://doi.org/10.1016/j.scitotenv.2024.177296, 2024.
- 833 Zhi, M. K., Wang, G. C., Xu, L., Li, K. I., Nie, W., Niu, H. Y., Shao, L. Y., Liu, Z. R., Yi, Z.W., Wang,
- Y. T., Shi, Z. B., Ito, A., Zhai, S. X., and Li, W. J.: How acid iron dissolution in aged dust particles
- responds to the buffering capacity of carbonate minerals during Asian dust storms. Environ. Sci.
- 836 Technol., 59(12): 6167–6178. https://doi.org/10.1021/acs.est.4c12370, 2025.

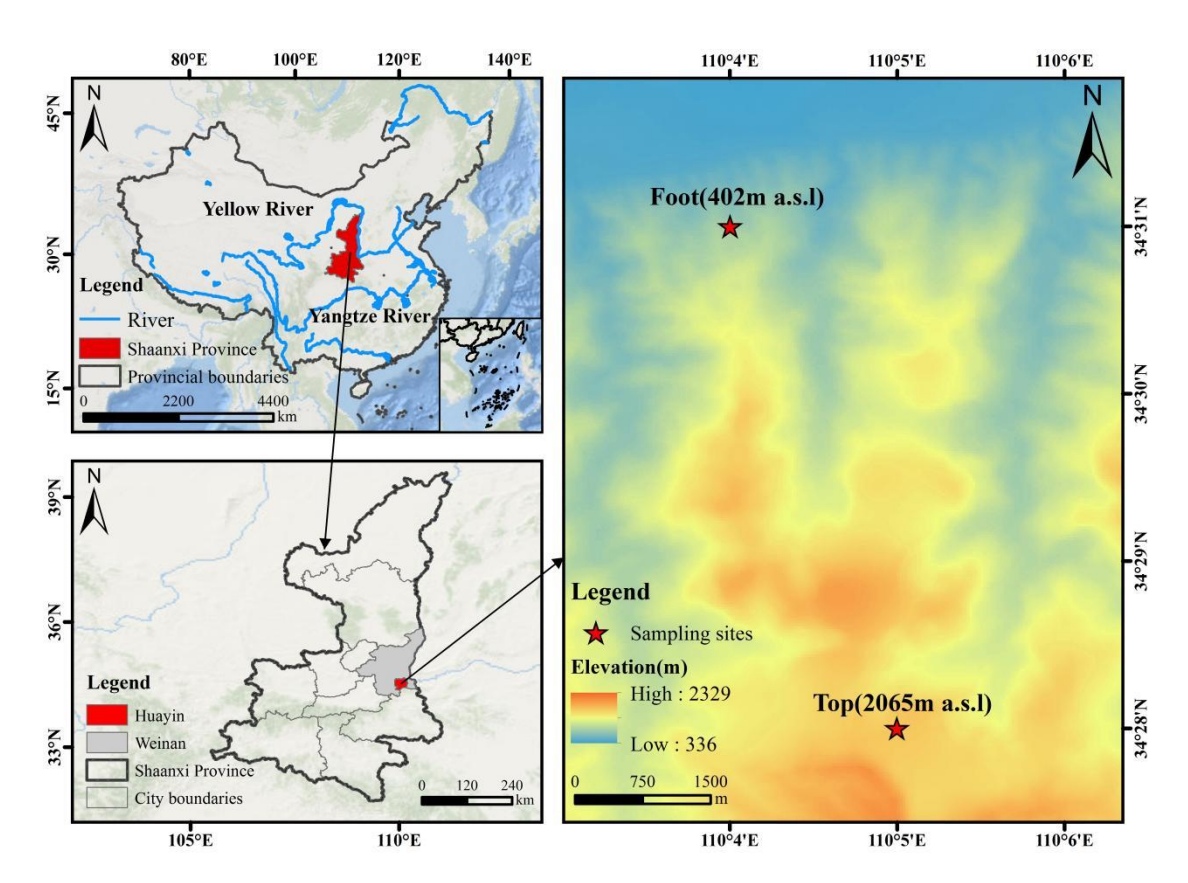


Figure 1 Distribution of aerosol sampling sites at the foot and top of Mount Hua (December 2020 to January 2021)

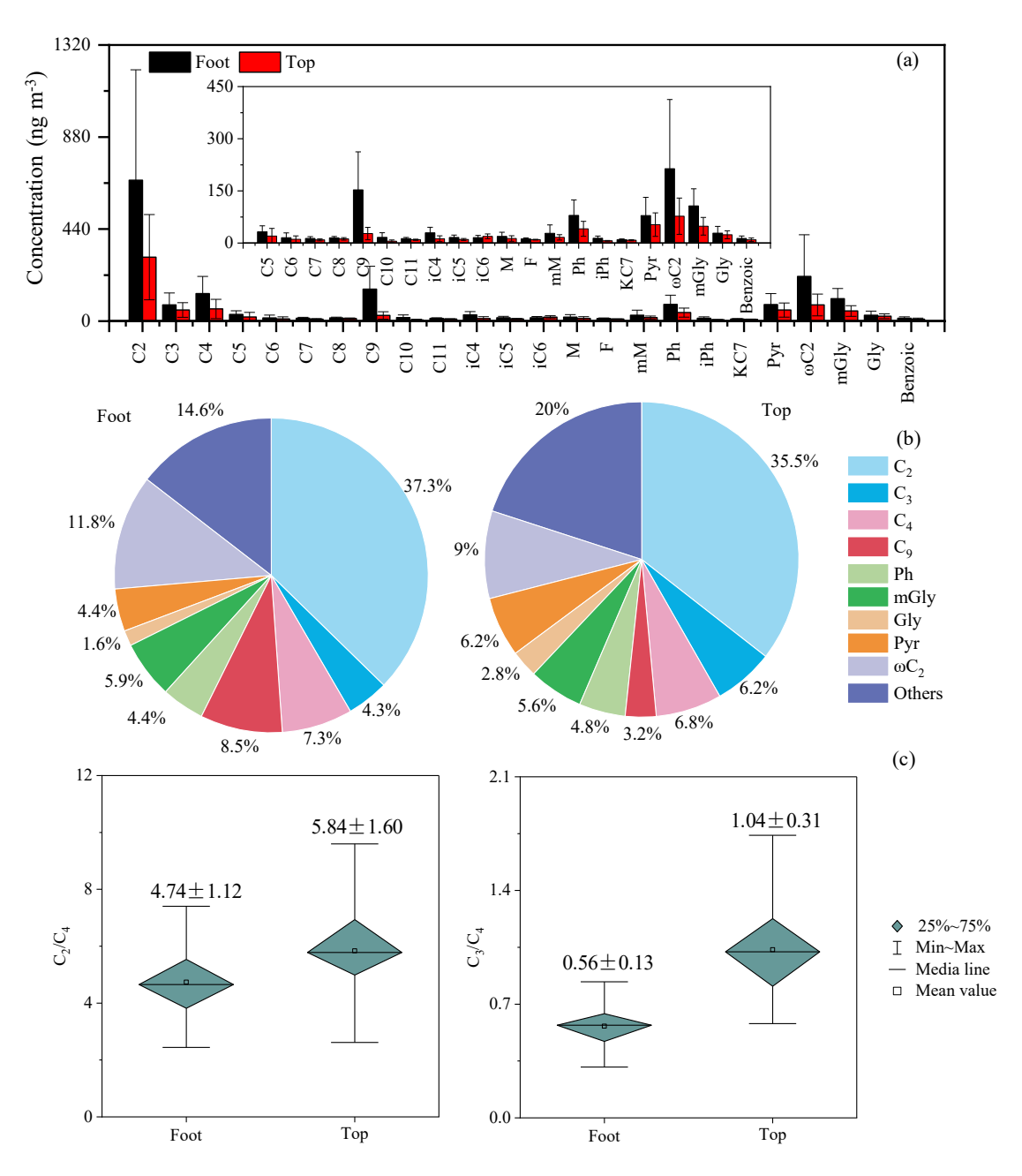


Figure 2 Molecular distribution of dicarboxylic acids and related Compounds (a), relative percentages of major dicarboxylic acids (b), and ratios of C_2/C_4 and C_3/C_4 (c) at the foot and top of Mount Hua during non-dust periods

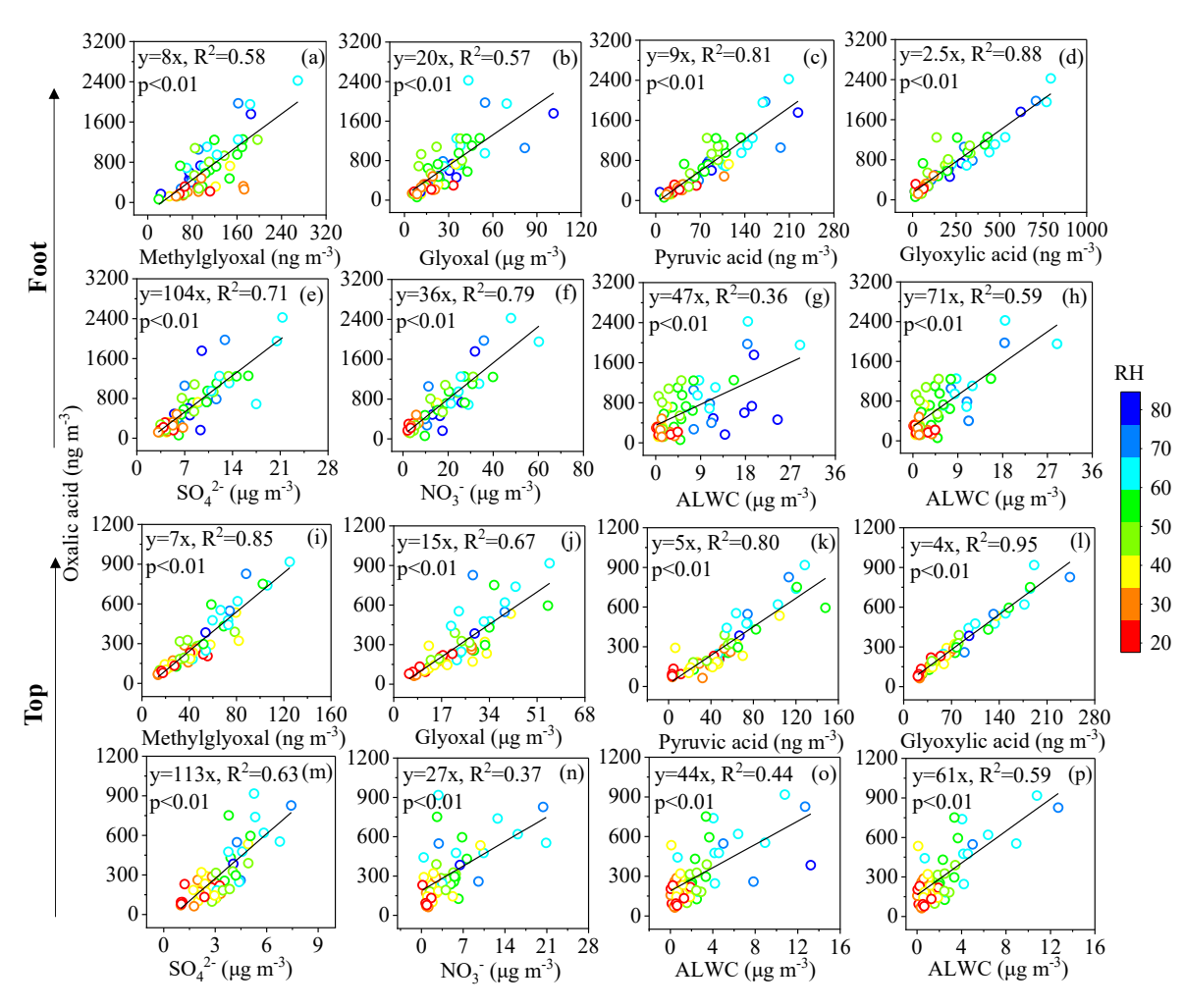


Figure 3 Correlation between C₂ and its key precursors, sulfate (SO₄²⁻), nitrate (NO₃⁻), and aerosol liquid water content (ALWC) at the foot and top of Mount Hua with varying relative humidity (RH)

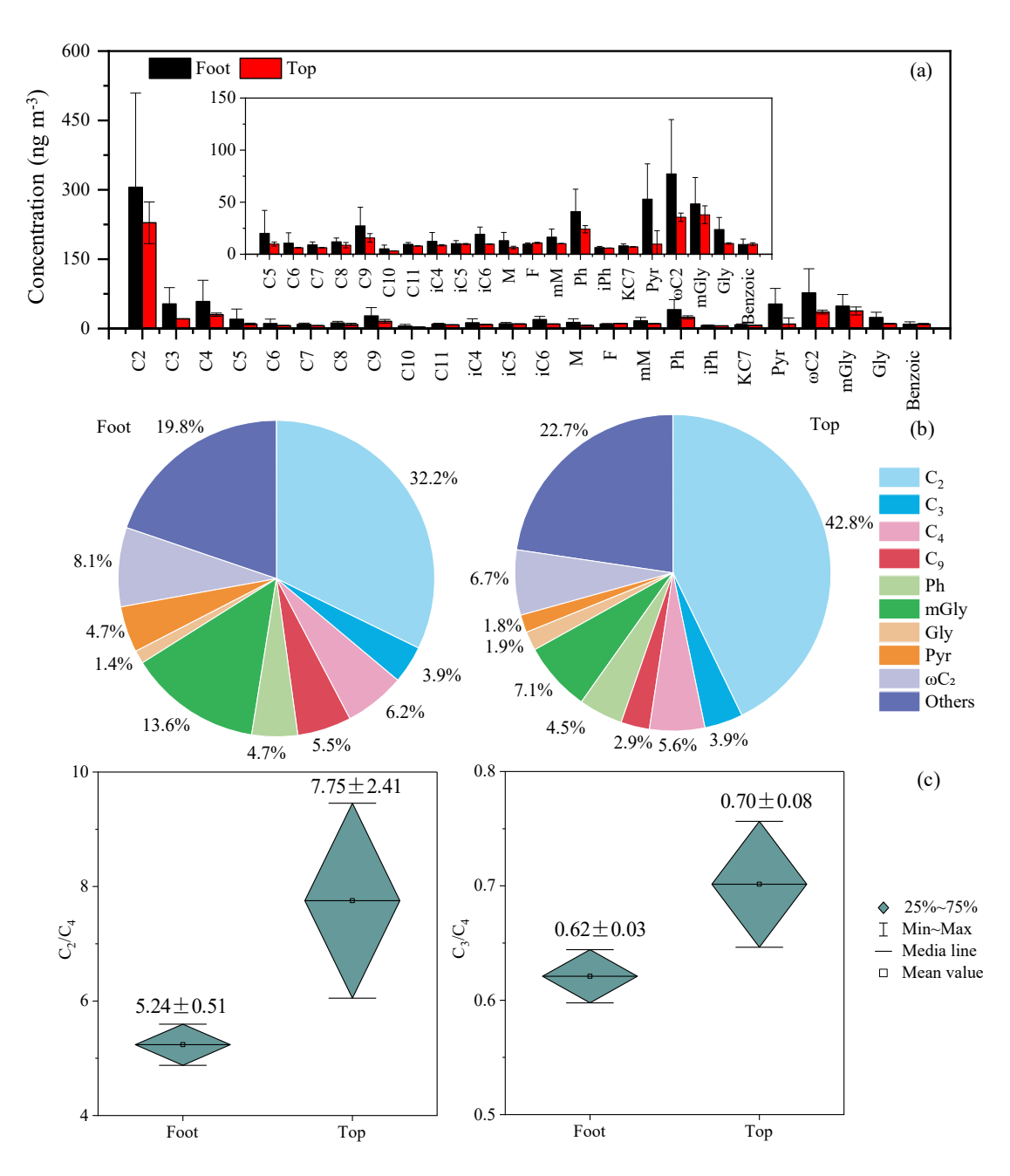


Figure 4 Molecular distribution of dicarboxylic acids and related compounds (a), relative percentages of major dicarboxylic acids (b), and ratios of C_2/C_4 and C_3/C_4 (c) at the foot and top of Mount Hua during dust events

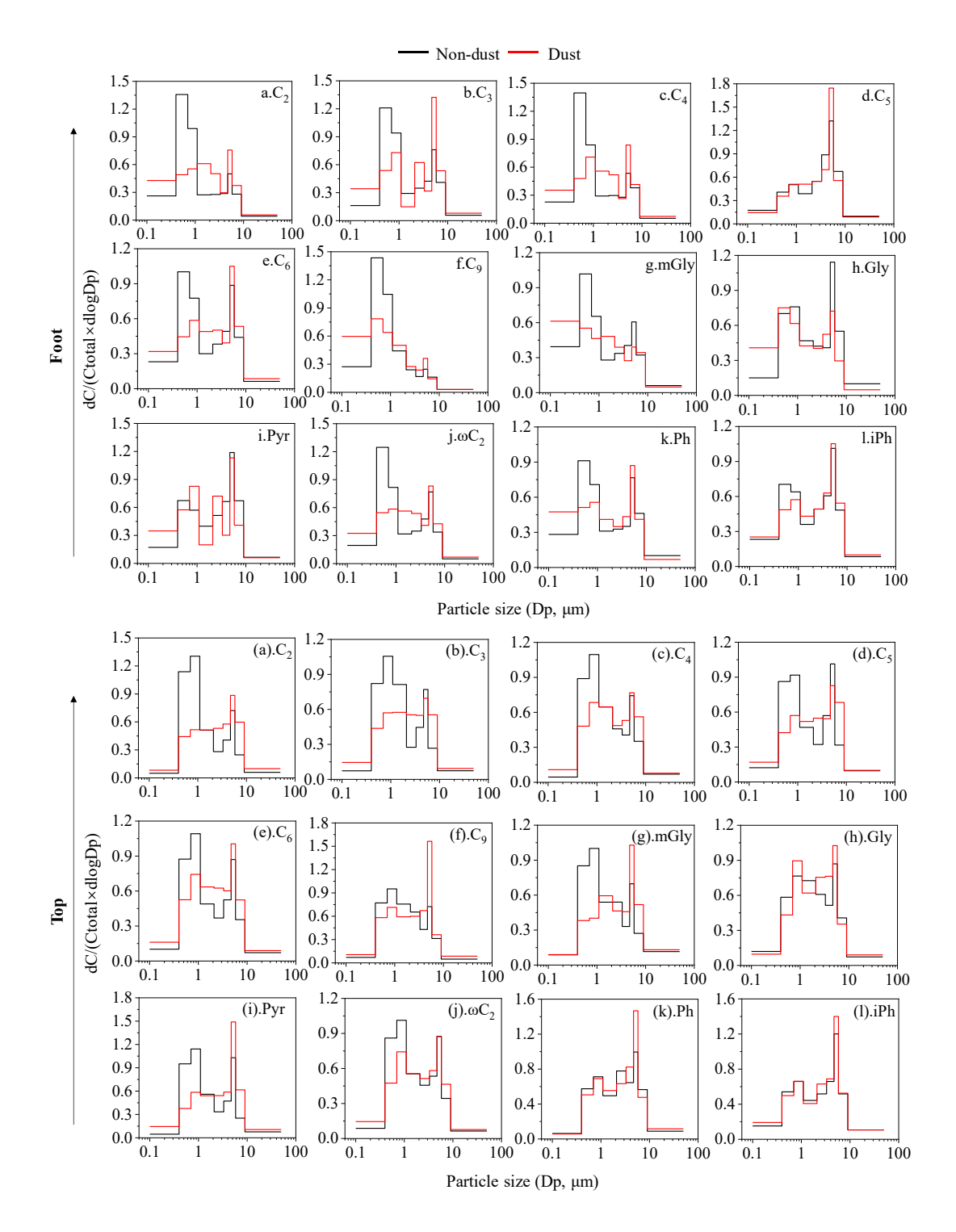


Figure 5 Size distribution of dicarboxylic acids at the foot and top of Mount Hua during non-dust and dust periods

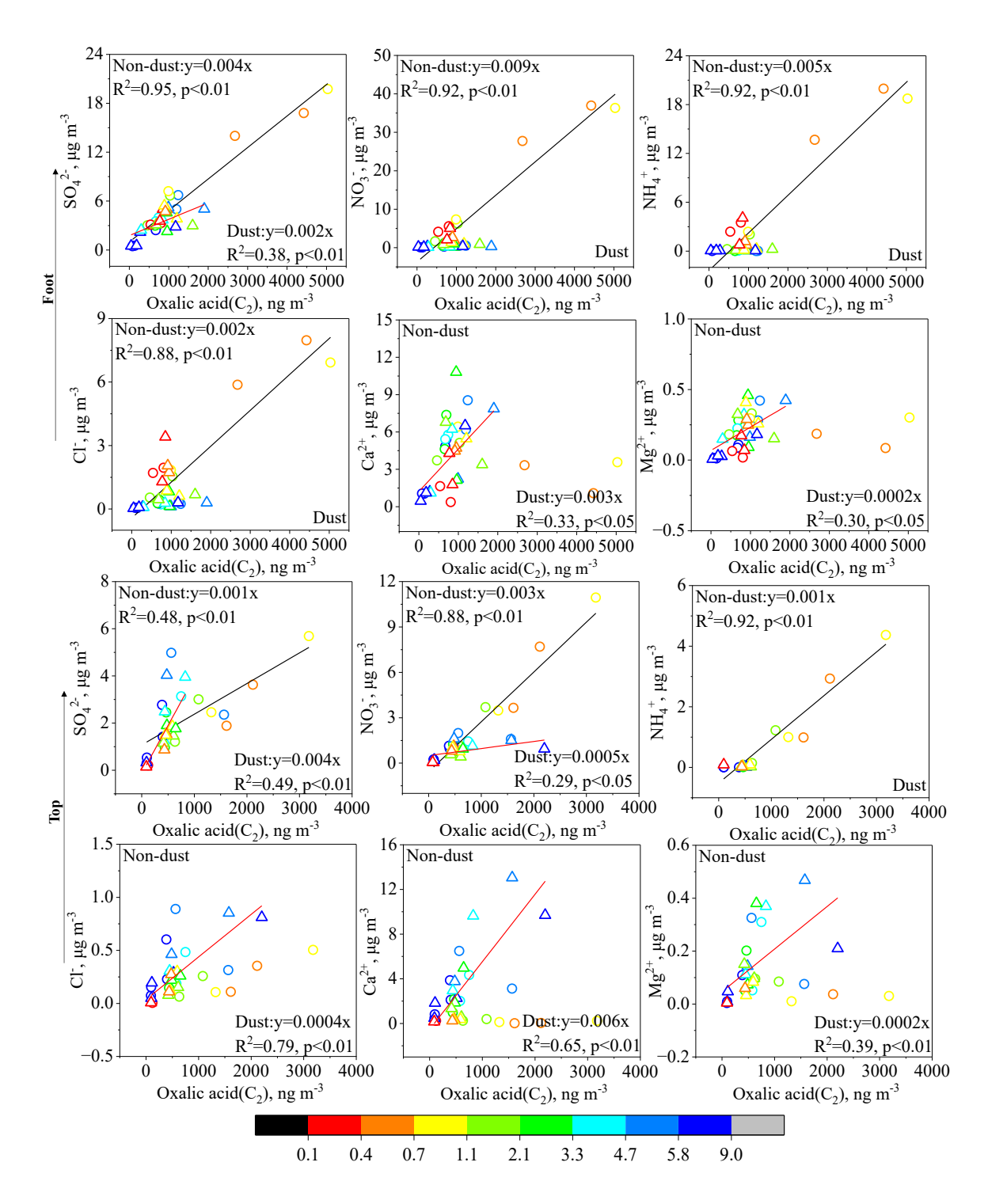


Figure 6 Correlation of C₂ with water-soluble ions at the foot and top of Mount Hua during non-dust and dust periods (Circles in the figure represent non-dust periods, and triangles represent dust periods)

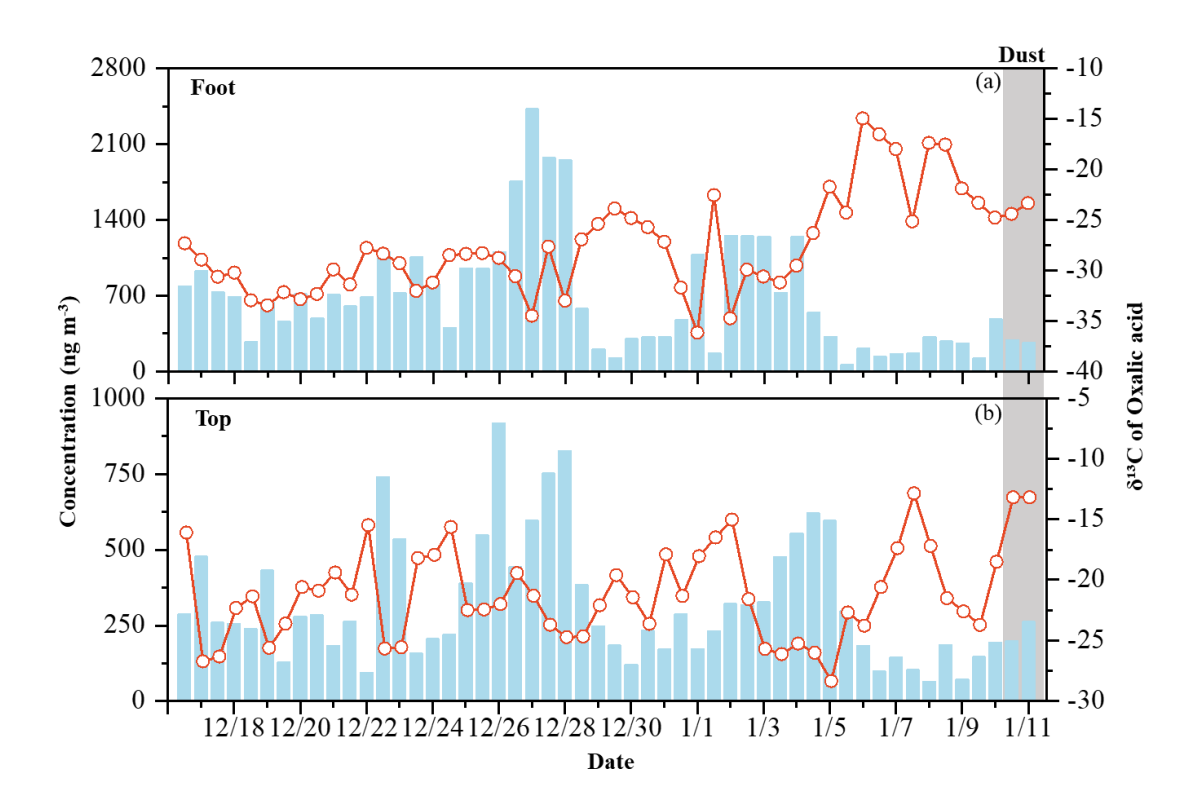


Figure 7 Stable carbon isotopes (δ¹³C) of C₂ in PM₂.5 at the foot and top of Mount Hua

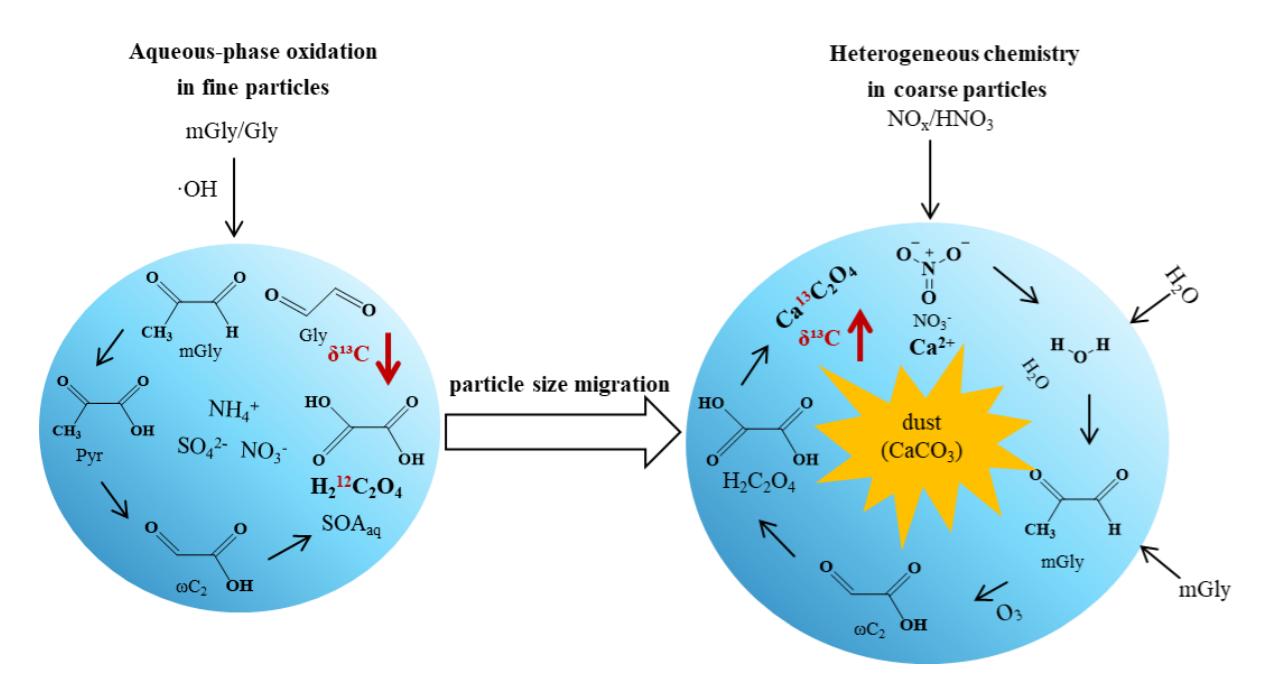


Figure 8 Mechanism diagram of dust-driven particle-size migration and formation pathways of C_2

Table 1 Average concentrations of dicarboxylic acids and related compounds in $PM_{2.5}$ at the foot and top of Mount Hua during non-dust periods

		Foot		Тор						
Compound	Daytime Nighttime Who			Daytime	Whole	R _{F/T}				
	(N = 26)	(N = 27)	(N = 53)	(N = 26)	(N = 27)	(N = 53)				
Dicarboxylic acids										
Oxalic, C ₂	766 ± 552	585 ± 497	674 ± 528	312 ± 224	299 ± 186	306 ± 204	2.2			
Malonic, C ₃	86 ± 58	71 ± 55	78 ± 56	54 ± 39	53 ± 32	53 ± 35	1.5			
Succinic, C ₄	152 ± 83	112 ± 77	132 ± 82	60 ± 47	57 ± 46	58 ± 46	2.3			
Glutaric, C ₅	38 ± 19	27 ± 14	32 ± 17	22 ± 27	18 ± 16	20 ± 22	1.6			
Adipic, C ₆	17 ± 15	14 ± 13	15 ± 14	12 ± 13	10 ± 6.3	11 ± 9.8	1.4			
Pimelic, C7	15 ± 5.0	12 ± 5.0	13 ± 5.1	9.2 ± 3.3	8.9 ± 2.3	9.0 ± 2.8	1.4			
Suberic, C ₈	16 ± 4.1	14 ± 3.4	15 ± 3.8	13 ± 3.7	12 ± 3.5	12 ± 3.6	1.3			
Azelaic, C9	175 ± 110	131 ± 106	153 ± 110	28 ± 19	27 ± 17	27 ± 18	5.7			
Sebacic, C ₁₀	19 ± 15	14 ± 11	16 ± 14	5.3 ± 3.5	5.3 ± 3.7	5.3 ± 3.5	3.0			
Undecanedioic, C ₁₁	14 ± 3.8	12 ± 2.5	13 ± 3.3	9.9 ± 1.8	9.2 ± 1.7	9.6 ± 1.8	1.4			
Methylmalonic, iC ₄	36 ± 17	24 ± 13	29 ± 16	13 ± 9.4	12 ± 7.6	13 ± 8.5	2.2			
Mehtylsuccinic, iC ₅	16 ± 5.4	16 ± 7.9	16 ± 6.7	10 ± 3.2	10 ± 2.4	10 ± 2.8	1.6			
Methylglutaric, iC ₆	18 ± 6.7	14 ± 5.4	16 ± 6.3	19 ± 7.7	19 ± 6.2	19 ± 6.9	0.8			
Maleic, M	22 ± 12	17 ± 11	19 ± 12	13 ± 10	13 ± 5.7	13 ± 7.9	1.5			
Fumaric, F	13 ± 3.4	11 ± 2.4	12 ± 3.0	10 ± 1.2	10 ± 1.0	9.7 ± 1.1	1.2			
Methylmaleic, mM	29 ± 18	27 ± 29	28 ± 24	17 ± 9.1	16 ± 6.2	16 ± 7.7	1.8			
Phthalic, Ph	89 ± 43	71 ± 45	80 ± 44	44 ± 23	39 ± 20	41 ± 22	2.0			
Isophthalic, iPh	15 ± 5.4	13 ± 7.0	14 ± 6.3	6.5 ± 1.2	6.5 ± 0.8	6.5 ± 1.0	2.2			
Ketopimelic, kC7	10.2 ± 2.3	9.4 ± 2.1	9.8 ± 2.2	8.3 ± 1.9	8.0 ± 1.7	8.1 ± 1.8	1.2			
		Keto	ocarboxylic ac	eids						
Pyruvic, Pyr	85 ± 45	73 ± 59	79 ± 53	52 ± 38	54 ± 30	53 ± 34	1.5			
Glyoxylic, ωC_2	230 ± 201	198 ± 200	214 ± 199	79 ± 58	75 ± 47	77 ± 52	2.8			
α-Dicarbonyls										
Glyoxal, Gly	29 ± 15	29 ± 23	29 ± 19	23 ± 13	24 ± 10	24 ± 12	1.2			
Methylglyoxal, mGly	128 ± 49	87 ± 42	107 ± 49	49 ± 28	48 ± 23	48 ± 25	2.2			
Others										
Benzoic, Ha	15 ± 7.1	12 ± 6.7	13 ± 6.9	9.6 ± 5.4	9.3 ± 5.1	9.4 ± 5.2	1.4			
Total detected (ng m ⁻³)	2029 ± 1294	1594 ± 1238	1807 ± 1280	879 ± 591	842 ± 481	860 ± 534	2.1			

Table 2 Average concentrations of dicarboxylic acids and related compounds in $PM_{2.5}$ at the foot and top of Mount Hua during dust events

		Foot		Тор					
Compound	Daytime	Nighttime	Whole	Daytime	Nighttime	Whole			
•	(N=1)	(N=1)	(N=2)	(N=1)	(N=1)	(N=2)			
Oxalic, C ₂	289	262	276 ± 20	261	197	229 ± 45			
Malonic, C ₃	28	38	33 ± 7.3	21	21	21 ± 0.1			
Succinic, C ₄	47	59	53 ± 8.9	28	33	30 ± 3.5			
Glutaric, C ₅	15	16	15 ± 0.5	8.4	11	10 ± 1.9			
Adipic, C ₆	9.8	10.2	10 ± 0.3	6.2	6.4	6.3 ± 0.2			
Pimelic, C ₇	7.6	9.2	8.4 ± 1.1	6.3	6.3	6.3 ± 0.0			
Suberic, C ₈	9.2	11	10 ± 1.3	6.9	11	8.7 ± 2.6			
Azelaic, C9	41	54	47 ± 9.4	13	19	16 ± 4.1			
Sebacic, C ₁₀	4.7	5.6	5.1 ± 0.7	3.2	3.2	3.2 ± 0.0			
Undecanedioic, C ₁₁	9.3	10	9.8 ± 0.7	8.0	7.9	8.0 ± 0.0			
Methylmalonic, iC ₄	15	16	16 ± 0.3	8.2	9.1	8.7 ± 0.6			
Mehtylsuccinic, iC5	12	11	12 ± 0.9	9.4	10.2	9.8 ± 0.6			
Methylglutaric, iC ₆	15	16	16 ± 0.3	9.5	10.0	9.8 ± 0.3			
Maleic, M	7.8	10	9.1 ± 1.8	7.3	5.6	6.4 ± 1.3			
Fumaric, F	13	15	14 ± 1.4	10.5	11.3	10.9 ± 0.6			
Methylmaleic, mM	12	13	13 ± 0.2	10.3	10.2	10.3 ± 0.0			
Phthalic, Ph	39	41	40 ± 1.3	22	27	24 ± 3.5			
Isophthalic, iPh	9.5	12	11 ± 1.6	5.9	5.9	5.9 ± 0.0			
Ketopimelic, kC7	7.5	7.9	7.7 ± 0.3	7.2	7.1	7.2 ± 0.1			
Pyruvic, Pyr	29	52	40 ± 17	0.6	19	9.8 ± 13			
Glyoxylic, ωC ₂	51	87	69 ± 26	33	38	36 ± 4.0			
Glyoxal, Gly	14	8.7	12 ± 4.1	9.8	10.9	10.4 ± 0.7			
Methylglyoxal, mGly	92	140	116 ± 34	32	44	38 ± 8.6			
Benzoic, Ha	12	17	15 ± 3.8	8.7	10.7	9.7 ± 1.4			
Total detected (ng m ⁻³)	761	949	855 ± 142	535	533	534 ± 92			

Table 3 Comparison of concentrations of dicarboxylic acids and related compounds in
particulate matter of different particle size ranges (≤2.1 μm and >2.1 μm) at the foot and top of

Mount Hua during non-dust and dust periods

	Foot					Тор						
C1	Non-dust Du		ust R _{D/N}		Non-dust		Dust		R _{D/N}			
Compound	≤2.1 µm	>2.1 μm	≤2.1 µm	>2.1 μm	≤2.1 μm	>2.1 μm	≤2.1 µm	>2.1 μm	≤2.1 μm	>2.1 μm	≤2.1 μm	>2.1 μm
Oxalic, C ₂	8662	2718	4880	2843	0.3	0.6	5512	2217	2161	2301	0.4	1.1
Malonic, C ₃	750	388	361	371	0.5	1.0	757	359	305	253	0.5	0.8
Succinic, C ₄	1505	594	829	505	0.4	0.6	986	488	371	294	0.5	0.8
Glutaric, C ₅	238	350	199	297	1.5	1.5	557	390	334	324	0.7	1.0
Adipic, C ₆	427	277	347	292	0.6	0.8	457	275	290	240	0.6	0.8
Azelaic, C9	2313	371	1097	304	0.2	0.3	646	302	379	396	0.5	1.0
Methylglyoxal, mGly	237	119	217	90	0.5	0.4	146	67	49	55	0.5	1.1
Glyoxal, Gly	312	268	237	145	0.9	0.6	192	129	140	114	0.7	0.8
Pyruvic, Pyr	729	800	687	513	1.1	0.7	1022	521	451	633	0.5	1.4
Glyoxylic, ωC ₂	2181	1171	979	663	0.5	0.7	1138	678	658	545	0.6	0.8
Phthalic, Ph	1018	652	499	386	0.6	0.8	564	481	302	356	0.9	1.2
Isophthalic, iPh (ng m ⁻³)	206	184	157	163	0.9	1.0	162	173	146	169	1.1	1.2